Available online at www.sciencedirect.com
ScienceDirect
ELSEVIER
Journal of Computational Physics 221 (2007) 439–468
JOURNAL OF COMPUTATIONAL PHYSICS
www.elsevier.com/locate/jcp

2D numerical simulation of the MEP energy-transport model with a finite difference scheme

V. Romano *

Dipartimento di Matematica e Informatica, Università di Catania, Viale A.Doria 6, I-95125 Catania, Italy

Received 9 March 2006; received in revised form 15 June 2006; accepted 17 June 2006
Available online 9 August 2006

Abstract

A finite difference scheme of Scharfetter–Gummel type is used to simulate a consistent energy-transport model for electron transport in semiconductors devices, free of any fitting parameters, formulated on the basis of the maximum entropy principle.

Simulations of silicon n^+–n–n^+ diodes, 2D-MESFET and 2D-MOSFET and comparisons with the results obtained by a direct simulation of the Boltzmann transport equation and with other energy-transport models, known in the literature, show the validity of the model and the robustness of the numerical scheme.
© 2006 Elsevier Inc. All rights reserved.

MSC: 35Q35; 65M06; 74F10

Keywords: Semiconductors; Energy-transport model; Finite differences; MESFET; MOSFET

1. Introduction

In today semiconductor technology, the miniaturization of devices is more and more progressing. As a consequence, the simulation of submicron semiconductor devices requires advanced transport models. Because of the presence of very high and rapidly varying electric fields, phenomena occur which cannot be described by means of the well-known drift-diffusion models, which do not incorporate energy as a dynamical variable. That is why some generalization has been sought in order to obtain more physically accurate models, like energy-transport and hydrodynamical models. The energy transport models which are implemented in commercial simulators are based on phenomenological constitutive equations for the particle flux and energy flux depending on a set of parameters which are fitted to homogeneous bulk material Monte Carlo simulations. However, a more satisfactory physical description should be based on relating the parameters appearing in the constitutive laws to the fundamental scattering properties of electrons with phonons and impurities [1]. In [2–4] a model free of any fitting parameters has been developed for the electron transport in silicon, where

* Fax: +39 095 330094.
E-mail address: romano@dmi.unict.it.

0021-9991/$ - see front matter © 2006 Elsevier Inc. All rights reserved.
doi:10.1016/j.jcp.2006.06.028

the parameters appearing in the constitutive laws are directly related to the collision operators of the semiclassical Boltzmann transport equation for electrons in semiconductors. Such a model is based on the maximum entropy principle (hereafter MEP), takes into account all the relevant scattering mechanisms in Silicon, i.e. scattering of electrons with acoustic and non-polar phonons and with impurities, and has been formulated also for non-parabolic bands. The model is represented, apart from the Poisson equation for the electric potential, by a hyperbolic quasilinear system of balance law. In [4], it has been shown that it is possible to recover an energy-transport limiting model which is equivalent in the stationary case to the original one, at least for smooth solutions.

This energy-transport model (hereafter MEP ET model) model has been tested in [5] both in one-dimensional problems, like n^+–n–n^+ diodes, and 2D problems, like a 2D MESFET and MOSFET, by using for the numerical integration a mixed finite element scheme [6,7] based on the lowest order Raviart–Thomas elements. This required the formulation of the model in terms of the dual entropy variables, that give rise to coupled nonlinear discretized equations whose numerical treatment must be done with great accuracy. In particular the choice of the mesh is crucial for the convergence of the scheme.

Here we formulate a numerical scheme suited for the MEP ET model which is based on an exponential fitting like that employed in the Scharfetter–Gummel scheme for the drift-diffusion model of semiconductors. The basic idea is to split the particle and energy density currents as the sum of two terms. Each of them is written by introducing suitable mean mobilities in order to get expressions of the currents similar to those arising in other energy-transport models known in the literature [8–12]. The original variables (density, energy and electric field) are used and a simple explicit discretization in time proves satisfactorily efficient avoiding the problem related to the high nonlinear coupling of the discretized equations of [5]. In fact as explained in detail in Section 3, the CFL condition on the time step, even if of parabolic type, is not very restrictive for reasonable meshes. The computational effort is comparable with that of the schemes in [5], retaining the same accuracy of the solution.

The method is very stable and robust and guarantees a good numerical current conservation.

A comparison with direct simulations of the Boltzmann equations for electron transport in semiconductors confirms the results obtained in [5] that the MEP one gives results that are more accurate with respect to the standard energy-transport models, usually employed in commercial simulators.

The numerical discretization of energy-transport models is itself an active area of research (the interested reader is referred to [13] for a complete review). A finite difference scheme based on a Scharfetter type discretization has been used in [14]. Finite difference schemes with entropy-decaying property have used in [15], while compact scheme of fourth-order have been employed in [16]. In [17] a mixed finite-volume techniques have been used. Apart the above mentioned article [6,7], other schemes based on the mixed finite elements have been used in [18,19]. They are based on the finite elements proposed in [20]. In [21] an adaptive formulation has been also given. The above mentioned schemes have been applied to the standard energy-transport known in the literature. Their application to the MEP energy-transport model requires major modification and it is an open problem.

The paper is organized as follows. In Section 2 we give a brief presentation of the model. In Section 3 the model is reformulated in terms of average mobilities and the numerical scheme is presented. In the remaining sections the validity of the model and robustness of the scheme is shown by simulating first a one-dimensional n^+–n–n^+ silicon diode and then, in the last two sections, a silicon MESFET and MOSFET in the two-dimensional case.

2. The MEP energy-transport model in the Kane dipersion relation case

In this section we give a sketch of the energy-transport model based on MEP. For more details the interested reader is referred to [2–4].

One assumes that the conduction band is described around each minimum (valley) by the Kane dispersion relation approximation

$$\mathscr{E}(\mathbf{k})[1+\alpha\mathscr{E}(\mathbf{k})]=\frac{\hbar^2k^2}{2m^*},\quad \mathbf{k}\in\mathbf{R}^3, \tag{1}$$

where $\mathscr{E}$ is the electron energy, m^* is the effective electron mass, $\hbar\mathbf{k}$ is the crystal momentum, $\hbar$ is the Planck constant divided by 2π and α is the non-parabolicity factor ($\alpha = 0.5\ \mathrm{eV}^{-1}$ for Silicon).

The energy-transport model, obtained for silicon semiconductor in [4,22] starting from the hydrodynamical model based on the maximum entropy principle [2,3], is given by the following set of balance equations for the electron density n and energy W, coupled to the Poisson equation for the electric potential ϕ

$$\frac{\partial n}{\partial t} + \operatorname{div}(n\mathbf{V}) = 0, \tag{2}$$

$$\frac{\partial (nW)}{\partial t} + \operatorname{div}(n\mathbf{S}) - nq\mathbf{V}\cdot\nabla\phi = nC_W, \tag{3}$$

$$\operatorname{div}(\epsilon\nabla\phi) = -q(N_\mathrm{D} - N_\mathrm{A} - n), \tag{4}$$

where N_D and N_A are the donor and acceptor densities respectively, q is the (positive) elementary charge, ϵ is the dielectric constant while div and ∇ are the divergence and gradient operators.

The evolution equations are closed with the constitutive relations for the velocity $\mathbf{V}$ and the energy-flux $\mathbf{S}$

$$\mathbf{V} = D_{11}(W)\nabla\log n + D_{12}(W)\nabla W + D_{13}(W)\nabla\phi, \tag{5}$$

$$\mathbf{S} = D_{21}(W)\nabla\log n + D_{22}(W)\nabla W + D_{23}(W)\nabla\phi. \tag{6}$$

The elements of the diffusion matrix $D = (D_{ij})$ read

$$D_{11} = \frac{c_{22}U - c_{12}F}{c_{11}c_{22} - c_{12}c_{21}}, \quad D_{12} = \frac{c_{22}U' - c_{12}F'}{c_{11}c_{22} - c_{12}c_{21}}, \quad D_{13} = -q\frac{c_{22} - c_{12}G}{c_{11}c_{22} - c_{12}c_{21}},$$

$$D_{21} = \frac{c_{11}F - c_{21}U}{c_{11}c_{22} - c_{12}c_{21}}, \quad D_{22} = \frac{c_{11}F' - c_{21}U'}{c_{11}c_{22} - c_{12}c_{21}}, \quad D_{23} = q\frac{c_{21} - c_{11}G^{(0)}}{c_{11}c_{22} - c_{12}c_{21}}.$$

All the coefficients c_{ij} and the functions U, F, G depend on the energy W. The prime denotes derivative with respect to W.

The energy production term has a relaxation form $C_W = -\frac{W-W_0}{\tau_W}$ where τ_W is the energy relaxation time, which depends also on W, and $W_0 = 3/2k_\mathrm{B}T_\mathrm{L}$ is the energy at equilibrium, with T_L the lattice temperature, here assumed to be constant.

The expressions of U, F, G, C_W, c_{ij}, D_{ij} have been obtained in [2,3] both for parabolic band and Kane's dispersion relation. In the case that the conduction energy bands of electrons are described by the Kane dispersion relation, the expressions of U, F, G C_W, c_{ij}, D_{ij} require a numerical evaluation of some integrals. These computations have been done in [2,3] and, in order to improve the efficiency of the simulation code, numerical tables have created for U, F, G C_W, c_{ij}, D_{ij}. In the code from the discrete data the values of interest are obtained by interpolation with splines. The integral expression of U, F, G C_W, c_{ij}, D_{ij} is reported for the sake of completeness in Appendix A along with the values of the physical parameters used in the simulations.

Here we report an important relation which will be of crucial importance in the sequel

Proposition 1

$$U = \frac{1}{\lambda^W}, \quad F = \frac{G}{\lambda^W}$$

where λ^W is the Lagrangian multiplier relative to the energy.

Remark. λ^W enters in the derivation of the model (the interested reader is referred to [23] and references therein). Its thermodynamical meaning is linked with the definition of non-equilibrium temperature T according to statistical mechanics

$$\lambda^W = \frac{1}{k_\mathrm{B}T},$$

where k_B is the Boltzmann constant.

The results we get with the MEP energy-transport model will be compared with those obtained by a deterministic simulation of the Boltzmann transport equations [24], the Stratton classical energy-transport model, which is employed in several commercial simulators, and the standard drift-diffusion one. Other energy-transport models have been also proposed [8,10–12] but as proved in [5] a comparison with Monte Carlo data shows that the Stratton one gives the best results.

For the sake of completeness we report also Stratton's energy-transport and drift-diffusion models in order to fix expression of the free parameters and function as mobilities and energy relaxation time.

In the Stratton model the energy is related to the electron absolute temperature T by the monatomic gas equation of state

$$W = \frac{3}{2} k_{\mathrm{B}} T,$$

while fluxes and energy relaxation time are given by

$$C_W = -\frac{\frac{3}{2}(k_{\mathrm{B}}T - k_{\mathrm{B}}T_{\mathrm{L}})}{\tau_W}, \tag{7}$$

$$n\mathbf{V} = -\tilde{\mu}_0 \left(\nabla n - \frac{en}{k_{\mathrm{B}}T} \nabla \phi \right), \tag{8}$$

$$n\mathbf{S} = -\frac{3}{2} \tilde{\mu}_0 [\nabla(k_{\mathrm{B}} n T) - en \nabla \phi], \tag{9}$$

where $\tilde{\mu}_0 = \frac{\mu_0 k_{\mathrm{B}} T_{\mathrm{L}}}{e}$. μ_0 is the low-field mobility and τ_W the energy relaxation time, usually taken as a constant.

In the simulations we set $\tau_W = 0.4$ ps, and $\mu_0 = 1400\ \mathrm{cm}^2/\mathrm{V\,s}$ that are the values more currently used in the literature [8–11].

From a theoretical point of view we remark that, apart the MEP model, all the other ones uses among the fundamental variables the absolute temperature T. This requires the knowledge on an equation of state relating T to the energy W and it is one of the more controversial question in non-equilibrium thermodynamics. W has a clear meaning at kinetic level as moment of the electron distribution function with respect to the weight function given by the electron microscopic energy [23], but only for parabolic band, neglecting the quadratic terms, the relation $W = \frac{3}{2} k_{\mathrm{B}} T$ is sound in analogy with monatomic gases. In the non-parabolic case, e.g. when the Kane dispersion relation is used, the equation of state relating T and W is given only implicitly as will be seen in the next section. This casts serious doubts on the appropriateness of the standard formulation of the energy-transport models which is not naturally generalizable to the non-parabolic case.

At last we report also the standard drift-diffusion model

$$\frac{\partial n}{\partial t} + \mathrm{div}(n\mathbf{V}) = 0, \tag{10}$$

$$\mathbf{J} = -D_n \nabla n + \mu_n \nabla \phi \tag{11}$$

with D_n diffusion coefficient and μ_n field-depend mobility.

We assume the validity of the Einstein relation

$$D_n = \mu_n \frac{k_{\mathrm{B}} T_0}{e}.$$

and use for the mobility the Caughey–Thomas formula [30]

$$\mu_n = \mu_0 \left[1 + \left(\frac{\mu_0 |\mathbf{E}|}{v_{\mathrm{s}}} \right)^2 \right]^{-1/2},$$

where the previous values of μ_0 is used for consistency while v_{s} is taken as 10^7 cm/s.

3. The numerical method

First we rewrite the current density $\mathbf{J} = n\mathbf{V}$ and the energy-flux density $\mathbf{H} = n\mathbf{S}$ given by

$$\mathbf{J} = D_{11}(W)\nabla n + nD_{12}(W)\nabla W + nD_{13}(W)\nabla\phi, \tag{12}$$

$$\mathbf{H} = D_{21}(W)\nabla n + nD_{22}(W)\nabla W + nD_{23}(W)\nabla\phi \tag{13}$$

as

$$\mathbf{J} = \mathbf{J}^{(1)} - \mathbf{J}^{(2)}, \quad \mathbf{H} = \mathbf{H}^{(1)} - \mathbf{H}^{(2)}, \tag{14}$$

where

$$\mathbf{J}^{(1)} = \frac{c_{22}}{D}[\nabla(nU) - qn\lambda^W U\nabla\phi], \quad \mathbf{J}^{(2)} = \frac{c_{12}}{D}[\nabla(nF) - qn\lambda^W F\nabla\phi], \tag{15}$$

$$\mathbf{H}^{(1)} = \frac{c_{11}}{D}[\nabla(nF) - qn\lambda^W F\nabla\phi], \quad \mathbf{H}^{(2)} = \frac{c_{12}}{D}[\nabla(nU) - qn\lambda^W U\nabla\phi] \tag{16}$$

with $D = c_{11}c_{22} - c_{12}c_{21}$.

The basic idea is to introduce suitable average mobilities that are constant in each cell so that $\mathbf{J}^{(i)}$ and $\mathbf{H}^{(i)}$, $i = 1, 2$, can be expressed by means of *local* Slotboom variables.

For the sake of clarity first we treat the one-dimensional case and then present the discretization in the two-dimensional case.

3.1. Discretization in one space dimension

Let us suppose that the equations are definite on the real interval $[0, L]$, with $L > 0$ the length of the device, and introduce the grid point $0 = x_0 < x_1 < \cdots x_i < \cdots x_{N-1} < x_N = L$, with N a positive integer. For simplicity we assume a uniform grid so $x_i = i\,h$ with $h = L/N$, and uniform time steps. Moreover we set $I_{i+1/2} = [x_i, x_{i+1}]$ and $x_{i\pm1/2} = x_i \pm h/2$. In the sequel the notation u_i^l will indicate the value of the variable $u(x,t)$ for $x = x_i$ and $t = l\Delta t$, l being a positive integer.

By replacing the partial derivatives with finite differences, the balance equations (2)–(4) can be discretized as

$$\frac{n_i^{l+1} - n_i^l}{\Delta t} + \frac{J_{i+1/2} - J_{i-1/2}}{h} + \mathrm{O}(h^2, \Delta t) = 0, \tag{17}$$

$$\frac{(nW)_i^{l+1} - (nW)_i^l}{\Delta t} + \frac{H_{i+1/2} - H_{i-1/2}}{h} - q\frac{J_{i+1/2} + J_{i-1/2}}{2}\,\frac{\phi_{i+1} - \phi_{i-1}}{2h} + \frac{3}{2}n_i\frac{W_i - W_0}{(\tau_W)_i} + \mathrm{O}(h^2, \Delta t) = 0, \tag{18}$$

$$\frac{1}{h^2}(\phi_{i+1} - 2\phi_i + \phi_{i-1}) + \frac{q}{\epsilon}(C_i - n_i) + \mathrm{O}(h^2) = 0, \tag{19}$$

where $C_i = N_\mathrm{D}(x_i) - N_\mathrm{A}(x_i)$. The variables with no temporal index must be considered evaluated at the time step $t = l\Delta t$. We remark that the discretization of Eq. (19) is valid for constant ϵ. It is straightforward to take into account a space dependent ϵ.

In order to complete the numerical scheme we must evaluate the current $J_{i+1/2}$ and $H_{i+1/2}$.

We approximate the electric potential ϕ by piece-wise linear function in each $I_{i+1/2}$

$$\phi(x) \simeq \phi_i + (x - x_i)\phi_{i+1}, \quad x \in I_{i+1/2}$$

and $c_{ij}(W)$ by functions that are constant on each interval $I_{i+1/2}$. This enable us to introduce the *local* mobilities, similar to those employed for other energy-transport models (see [13,25])

$$g_{11} = -\frac{c_{22}}{D}, \quad g_{12} = -\frac{c_{12}}{D}, \tag{20}$$

$$g_{21} = -\frac{c_{11}}{D}, \quad g_{21} = -\frac{c_{12}}{D} \tag{21}$$

and write the significant components of $\mathbf{J}^{(i)}$ and $\mathbf{H}^{(i)}$ as

$$J^{(i)} \simeq -\frac{\partial g_{1i}}{\partial x} + q\overline{\lambda}^W g_{1i}\frac{\partial\phi}{\partial x}, \tag{22}$$

$$H^{(i)} \simeq -\frac{\partial g_{2i}}{\partial x} + q\overline{\lambda}^W g_{2i}\frac{\partial \phi}{\partial x}, \tag{23}$$

where $\overline{\lambda}^W$ is the cell mean value of λ^W, we approximate as

$$\overline{\lambda}^W \simeq \frac{1}{2}\left[\lambda^W(W_i) + \lambda^W(W_{i+1})\right]. \tag{24}$$

After introducing $U_T = 1/q\lambda^W$, which plays the role of a thermal potential, and indicating by $\overline{U}_T$ its constant approximation in each cell $I_{i+1/2}$, it is possible to define the *local* Slotboom variables

$$s_{kr} = \exp(-\phi/\overline{U}_T)g_{kr}$$

that satisfy

$$\frac{\partial s_{1r}}{\partial x} \simeq -\exp(-\phi/\overline{U}_T)J^{(r)}, \tag{25}$$

$$\frac{\partial s_{2r}}{\partial x} \simeq -\exp(-\phi/\overline{U}_T)H^{(r)}. \tag{26}$$

In each cell $I_{i+1/2}$ we can express $J^{(r)}$ as a Taylor expansion

$$J^{(r)}(x) = J^{(r)}_{i+1/2} + (x - x_{i+1/2})\left(\frac{\partial J^{(r)}}{\partial x}\right)_{x_{i+1/2}} + \mathrm{O}(h^2). \tag{27}$$

By integrating (25) and (26) over $I_{i+1/2}$ we find up to $\mathrm{O}(h^2)$

$$(s_{1r})_{i+1} - (s_{1r})_i = -\int_{x_i}^{x_{i+1}} \exp(-\phi/\overline{U}_T)J^{(r)}_{i+1/2}\,\mathrm{d}x.$$

By taking into account that $\phi(x)$ is linear in $I^{(r)}_{i+1/2}$, the last integral can be evaluated, obtaining

$$J^{(r)}_{i+1/2} = \frac{\phi_{i+1} - \phi_i}{\overline{U}_T}\left(\mathrm{e}^{-\phi_{i+1}/\overline{U}_T} - \mathrm{e}^{-\phi_{i+1}/\overline{U}_T}\right)^{-1}$$

which, after some elementary algebra can be written as

$$J^{(r)}_{i+1/2} = -z\coth z\frac{(g_{1r})_{i+1} - (g_{1r})_i}{h} + z\frac{(g_{1r})_{i+1} + (g_{1r})_i}{h}, \quad r = 1,2 \tag{28}$$

with $z = \frac{\phi_{i+1}-\phi_i}{2\overline{U}_T}$. If $z = 0$, that is if $\phi_{i+1} = \phi_i$, the previous expression remains valid provided that $z\coth z$ is replaced with the limit as $z \mapsto 0$ which is equal to one.

Similarly for the energy density current one finds

$$H^{(r)}_{i+1/2} = -z\coth z\frac{(g_{2r})_{i+1} - (g_{2r})_i}{h} + z\frac{(g_{2r})_{i+1} + (g_{2r})_i}{h}, \quad r = 1,2. \tag{29}$$

Formulas (28) and (29) are nonlinear exponential fittings similar to that introduced by Scharfetter and Gummel for the drift-diffusion equations (see [26]).

The complete numerical scheme is summarized below

$$n_i^{l+1} = n_i^l - \Delta t\frac{J_{i+1/2} - J_{i-1/2}}{h} = 0, \tag{30}$$

$$(nW)_i^{l+1} = (nW)_i^l - \Delta t\left[\frac{H_{i+1/2} - H_{i-1/2}}{h} - q\frac{J_{i+1/2} + J_{i-1/2}}{2}\,\frac{V_{i+1} - V_{i-1}}{2h} + \frac{3}{2}n_i\frac{W_i - W_0}{(\tau_W)_i}\right], \tag{31}$$

$$\frac{1}{h^2}\left(\phi_{i+1} - 2\phi_i + \phi_{i-1}\right) + \frac{q}{\epsilon}(C_i - n_i) = 0, \tag{32}$$

$$J_{i+1/2} = J^{(1)}_{i+1/2} - J^{(2)}_{i+1/2}, \quad H_{i+1/2} = H^{(1)}_{i+1/2} - H^{(2)}_{i+1/2}, \tag{33}$$

$$J^{(r)}_{i+1/2} = -z\coth z\frac{(g_{1r})_{i+1} - (g_{1r})_i}{h} + z\frac{(g_{1r})_{i+1} + (g_{1r})_i}{h}, \quad r = 1,2, \tag{34}$$

$$H^{(r)}_{i+1/2} = -z\coth z\frac{(g_{2r})_{i+1} - (g_{2r})_i}{h} + z\frac{(g_{2r})_{i+1} + (g_{2r})_i}{h}, \quad r = 1,2 \tag{35}$$

supplemented with a CFL condition $\Delta t/(\Delta x)^2 < c$, where c is a suitable positive constant.

Remark. The theoretical value of the constant c is difficult to obtain in an explicit way. Estimations have been obtained with numerical experiments, but a rough idea of the numerical value of c can be deduced from the drift-diffusion limit model (10) in the linear approximation where the classical parabolic condition

$$\frac{D_n\Delta t}{(\Delta x)^2} < \frac{1}{2}$$

holds.

If we express the time in picoseconds and the length in μm, for a mesh of 100 points in a device of 0.1 μm, one has in such units $\Delta x = 10^{-3}$ and the CFL condition reads

$$\Delta t < 0.138 \times 10^{-3} = 0.138\Delta x$$

(we recall that $D_n = \frac{\mu_0 k_B T_L}{3}$ and set $\mu_0 = 1400\ \text{cm}^2/\text{V s}$ and $k_B T/e = 0.0259\ \text{eV}$). Therefore for grids which are not too fine, practically the CFL condition is as that of hyperbolic type. Since the two diffusion coefficients in the energy-transport model are of the same order of D_n, this justifies the efficiency of the simple explicit scheme in time.

The following proposition gives an estimate of the truncation error for smooth solutions.

Proposition 2. *The leading truncation errors R_1 and R_2 in Eqs.* (30) *and* (31), *respectively*, *satisfy for sufficiently regular solutions the estimates*

$$|R_1| \leqslant O(h^2)\max_{x\in[0,L]}\left|\frac{\partial^3 J}{\partial x^3}\right| + O(\Delta t), \tag{36}$$

$$|R_2| \leqslant O(h^2)\max\left(\max_{x\in[0,L]}\left|\frac{\partial^2 J}{\partial x^2}\right|, \max_{x\in[0,L]}\left|\frac{\partial^3 H}{\partial x^3}\right|, \frac{q}{\epsilon}\max_{x\in[0,L]}\left|\frac{\partial}{\partial x}(n-C)\right|\right) + O(\Delta t), \tag{37}$$

where $O(h^2)$ *is a positive term of second order in h and* $O(\Delta t)$ *a positive term of first order in* Δt.

Proof. The estimates are consequence of the elementary relations

$$\frac{J^{(r)}_{i+1/2} + J^{(r)}_{i-1/2}}{2} = J^{(r)}(x_i) + \frac{1}{8}h^2\left(\frac{\partial^2 J^{(r)}}{\partial x^2}\right)_{x_i} + O(h^3),$$

$$\frac{\phi_{i+1} - \phi_{i-1}}{2h} = -E(x_i) - \frac{1}{6}h^2\left(\frac{\partial^2 E}{\partial x^2}\right)_{x_i} + O(h^3)$$

and the more accurate approximations

$$J^{(r)}_{i+1/2} = -z\coth z\frac{(g_{1r})_{i+1} - (g_{1r})_i}{h} + z\frac{(g_{1r})_{i+1} + (g_{1r})_i}{h} + O(h^2)\left(\frac{\partial^2 J^{(r)}}{\partial x^2}\right)_{x_{i+1/2}}, \quad r = 1,2,$$

$$H^{(r)}_{i+1/2} = -z\coth z\frac{(g_{2r})_{i+1} - (g_{2r})_i}{h} + z\frac{(g_{2r})_{i+1} + (g_{2r})_i}{h} + O(h^2)\left(\frac{\partial^2 H^{(r)}}{\partial x^2}\right)_{x_{i+1/2}}, \quad r = 1,2. \qquad \square$$

3.2. Discretization in two space dimension

The previous scheme can be generalized in order to deal with two-dimensional space problems. We introduce the grid points (x_i, y_j) with $x_{i+1} - x_i = h = \text{constant}$ and $y_{j+1} - y_j = k = \text{constant}$, and the middle points $(x_i, y_{j\pm1/2}) = (x_i, y_j \pm k/2)$ and $(x_{i\pm1/2}, y_j) = (x_i \pm h/2, y_j)$. A uniform time step Δt is used and we set $u^l_{i,j} = u(x_i, y_j, l\Delta t)$ as in the one space dimension.

By indicating with J_x and J_y the x- and y-component of the current density $\mathbf{J}$ and by H_x and H_y the x- and y-component of $\mathbf{H}$, we discretized the balance equations (2)–(4) in the bidimensional case as

$$\frac{n_i^{l+1}-n_i^l}{\Delta t}+\frac{(J_x)_{i+1/2,j}-(J_x)_{i-1/2,j}}{h}+\frac{(J_y)_{i,j+1/2}-(J_y)_{i,j-1/2}}{k}+\mathrm{O}(h^2,k^2,\Delta t)=0, \tag{38}$$

$$\begin{aligned}&\frac{(nW)_i^{l+1}-(nW)_i^l}{\Delta t}+\frac{(H_x)_{i+1/2,j}-(H_x)_{i-1/2,j}}{h}+\frac{(H_y)_{i,j+1/2}-(H_y)_{i,j-1/2}}{k}\\&\quad-q\frac{(J_x)_{i+1/2,j}+(J_x)_{i-1/2,j}}{2}\frac{\phi_{i+1,j}-\phi_{i-1,j}}{2h}-q\frac{(J_y)_{i,j+1/2}+(J_y)_{i,j-1/2}}{2}\frac{\phi_{i,j+1}-\phi_{i,j-1}}{2k}\\&\quad+\frac{3}{2}n_{i,j}\frac{W_{i,j}-W_0}{(\tau_W)_{i,j}}+\mathrm{O}(h^2,k^2,\Delta t)=0,\end{aligned} \tag{39}$$

$$\frac{1}{h^2}\left(\phi_{i+1,j}-2\phi_{i,j}+\phi_{i-1,j}\right)+\frac{1}{k^2}\left(\phi_{i,j+1}-2\phi_{i,j}+\phi_{i,j-1}\right)+\frac{q}{\epsilon}(C_{i,j}-n_{i,j})+\mathrm{O}(h^2,k^2)=0. \tag{40}$$

The variables without temporal index must be considered evaluated at time level l.

Again we need the values of the components of the currents in the middle points. Let us introduce the sets (see Fig. 1)

$$I_{i+1/2,j}=[x_i,x_{i+1}]\times[y_{j-1/2},y_{i,j+1/2}],\quad I_{i,j+1/2}=[x_{i-1/2},x_{i+1/2}]\times[y_j,y_{j+1}]$$

and expand $J_x^{(r)}$, $r=1,2$, in Taylor's series in $I_{i+1/2,j}$

$$J_x^{(r)}(x,y)=(J_x^{(r)})_{i+1/2,j}+(x-x_{i+1/2})\left(\frac{\partial J_x^{(r)}}{\partial x}\right)_{i+1/2,j}+(y-y_j)\left(\frac{\partial J_x^{(r)}}{\partial y}\right)_{i+1/2,j}+\mathrm{O}(\Delta x,\Delta y)$$

and $J_y^{(r)}$, $r=1,2$, in Taylor's series in $I_{i,j+1/2}$

$$J_y^{(r)}(x,y)=(J_y^{(r)})_{i,j+1/2}+(x-x_i)\left(\frac{\partial J_y^{(r)}}{\partial x}\right)_{i,j+1/2}+(y-y_{j+1/2})\left(\frac{\partial J_y^{(r)}}{\partial y}\right)_{i,j+1/2}+\mathrm{O}(\Delta x,\Delta y).$$

In terms of the Slotboom variables one can write

$$\nabla s_{1r}\simeq-\exp(-\phi/\overline{U}_T)\mathbf{J}^{(r)},\quad \nabla s_{2r}\simeq-\exp(-\phi/\overline{U}_T)\mathbf{H}^{(r)},\quad r=1,2. \tag{41}$$

From the x-component of $(41)_1$, one has

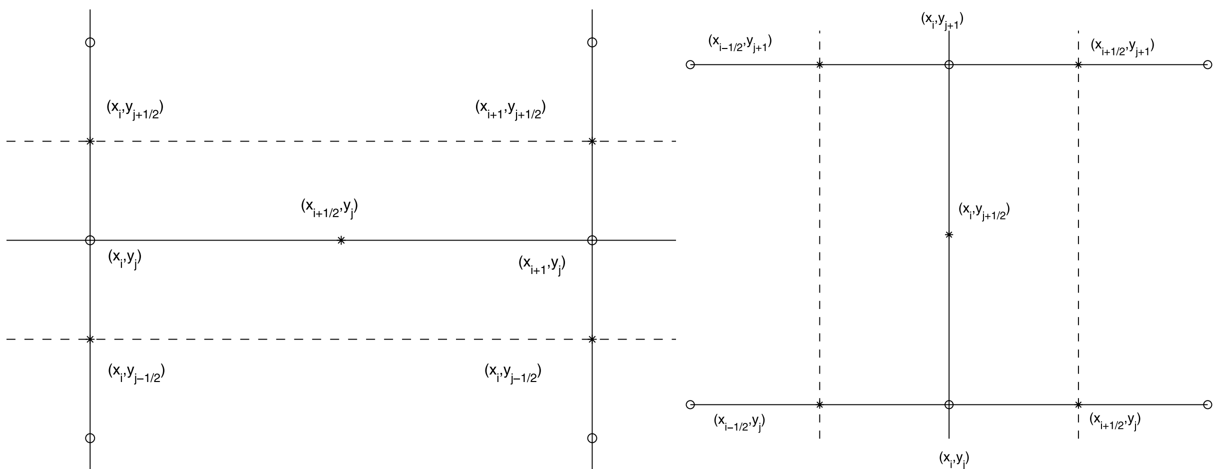

Fig. 1. Stencil for the evaluation of the currents. On the left the set $I_{i+1/2,j}$, on the right the set $I_{i,j+1/2}$. The currents are evaluated at the grid points denoted with $*$.

$$\frac{\partial s_{1r}(x,y_j)}{\partial x} \simeq -\exp(-\phi/\overline{U}_T) J_x^{(r)}(x,y_j)$$
$$= -\exp(-\phi/\overline{U}_T)\left\{ (J_x^{(r)})_{i+1/2,j} + (x - x_{i+1/2}) \left(\frac{\partial J_x^{(r)}}{\partial x}\right)_{i+1/2,j} + \mathrm{O}(\Delta x, \Delta y) \right\}, \tag{42}$$

which, after integration over $[x_i, x_{i+1}]$ and some algebra similar to that of the one space dimensional case, gives

$$(J_x^{(r)})_{i+1/2,j} = -z_{i+1/2,j} \coth z_{i+1/2,j} \frac{(g_{1r})_{i+1,j} - (g_{1r})_{i,j}}{h} + z_{i+1/2,j} \frac{(g_{1r})_{i+1,j} + (g_{1r})_{i,j}}{h}, \quad r = 1,2, \tag{43}$$

where $z_{i+1/2,j} = \frac{\phi_{i+1,j} - \phi_{i,j}}{2\overline{U}_T}$.

Likewise by evaluating the y-component of (41)$_2$ and integrating over $[y_j, y_{j+1}]$ we find

$$(J_y^{(r)})_{i,j+1/2} = -z_{i,j+1/2} \coth z_{i,j+1/2} \frac{(g_{1r})_{i,j+1} - (g_{1r})_{i,j}}{k} + z_{i,j+1/2} \frac{(g_{1r})_{i,j+1} + (g_{1r})_{i,j}}{k}, \quad r = 1,2, \tag{44}$$

where $z_{i,j+1/2} = \frac{\phi_{i,j+1} - \phi_{i,j}}{2\overline{U}_T}$. With the same procedure the following discrete expression for the components of the energy flux are obtained:

$$(H_x^{(r)})_{i+1/2,j} = -z_{i+1/2,j} \coth z_{i+1/2,j} \frac{(g_{2r})_{i+1,j} - (g_{2r})_{i,j}}{h} + z_{i+1/2,j} \frac{(g_{2r})_{i+1,j} + (g_{2r})_{i,j}}{h}, \tag{45}$$

$$(H_y^{(r)})_{i,j+1/2} = -z_{i,j+1/2} \coth z_{i,j+1/2} \frac{(g_{2r})_{i,j+1} - (g_{2r})_{i,j}}{k} + z_{i,j+1/2} \frac{(g_{2r})_{i,j+1} + (g_{2r})_{i,j}}{k}, \quad r = 1,2. \tag{46}$$

The error in formulas (43)–(46) is $\mathrm{O}(h,k)$.

Remark. In the bidimensional case the discretization of the Poisson equation leads to a linear algebraic system whose structure depends on the specific boundary conditions one is dealing with. Some standard methods can be used (e.g. see [27]), but an accurate treatment is needed to achieve a good convergence rate. A practical alternative is to use a false transient method which consists in replacing the original Poisson equation with the time dependent one

$$\phi_t - \mathrm{div}(\epsilon \nabla \phi) = q(N_{\mathrm{D}} - N_{\mathrm{A}} - n). \tag{47}$$

The solution of (47) as $t \mapsto +\infty$ is the same as that of the original Poisson equation, at least in the smooth case.

If we introduce a time step $\Delta\hat{t}$ e set $\phi_{ij}^r = \phi(x_i, y_j, r\Delta\hat{t})$, (47) can be discretized in an explicit way as

$$\phi_{ij}^{r+1} = \phi_{ij}^r + \epsilon\Delta\hat{t}\left[\frac{1}{h^2}(\phi_{i+1,j} - 2\phi_{i,j} + \phi_{i-1,j}) + \frac{1}{k^2}(\phi_{i,j+1} - 2\phi_{i,j} + \phi_{i,j-1}) + q(C_{i,j} - n_{i,j})\right] \tag{48}$$

with the notable advantage to take easily into account the different types of boundary conditions, that will be considered in more detail in the next sections. The price to pay is that at each time step, we need to reach the stationary state of (47) by using a time step satisfying the CFL condition, usual for parabolic equations,

$$\Delta\hat{t} \leqslant \frac{1}{2} \frac{1}{\frac{1}{h^2} + \frac{1}{k^2}}.$$

However the computational effort is comparable with that required by direct methods.

4. Simulation of a n$^+$–n–n$^+$ silicon diode

We start to test the numerical validity of our scheme with problems in one space dimension, simulating a ballistic n$^+$–n–n$^+$ silicon diode. The n$^+$ regions are 0.1 μm long with a doping density of 10^{18} cm^{-3}, the doping density in n-region is 10^{16} cm^{-3}, the applied voltage is 1 V while the channel has different lengths: 0.2, 0.05 and 0.025 μm. These cases are challenging tests because quantum corrections should be still negligible [28] and a semiclassical transport description still accurate. Moreover it is important to observe that several quantum

macroscopic models, e.g. the quantum drift-diffusion or energy-transport ones, are obtained by adding additional terms to the classical counterpart. Therefore this latter must be already accurate at a semiclassical level.

As boundary conditions we impose, as usual for ohmic contacts, that the density equals the doping and set the voltage equal to zero and to the bias voltage in the right and left boundaries, respectively. Concerning the energy we do not require that it assumes the equilibrium value, but impose homogeneous Newmann condition at the edges of the devices because this choice leads to results in better agreement with a direct integration of the Boltzmann equation.

The first case is that with the channel 0.2 μm long. The stationary regime is reached after about 5 ps. Since high nonlinearities are present in the scheme, the effective spacial order of convergence can be determined only numerically. To this end meshes with 48, 96, 192 and 384 cells have been considered. By denoting with $u_i^{(A)}$, $A = 1, 2, 3, 4$ the numerical values of the generic variable u at the grid point i, obtained with 48, 96, 192 and 384 cells at the stationary regime, the order of convergence p, estimated as

$$\frac{1}{\log 2} \log \frac{\|n_{\mathrm{i}}^{(A)} - n_{\mathrm{i}}^{(A+2)}\|_\infty}{\|n_{\mathrm{i}}^{(A+1)} - n_{\mathrm{i}}^{(A+2)}\|_\infty}$$

has been reported in Table 1. For each variable (density, energy and potential) two estimation of p are indicated: one by comparing the solutions with 48, 96 and 192 grid points, the other by comparing the solutions with 96, 192 and 384 grid points. Although a full second-order accuracy is not reached, the scheme is robust and guarantees a superlinear convergence rate whose mean value is about 1.5.

Table 1
Order of convergence for each variable, by comparing several meshes

Meshes	Density	Energy	Potential
48, 96, 192	1.3716	1.5050	1.4398
96, 192, 384	1.5899	1.5572	1.5212

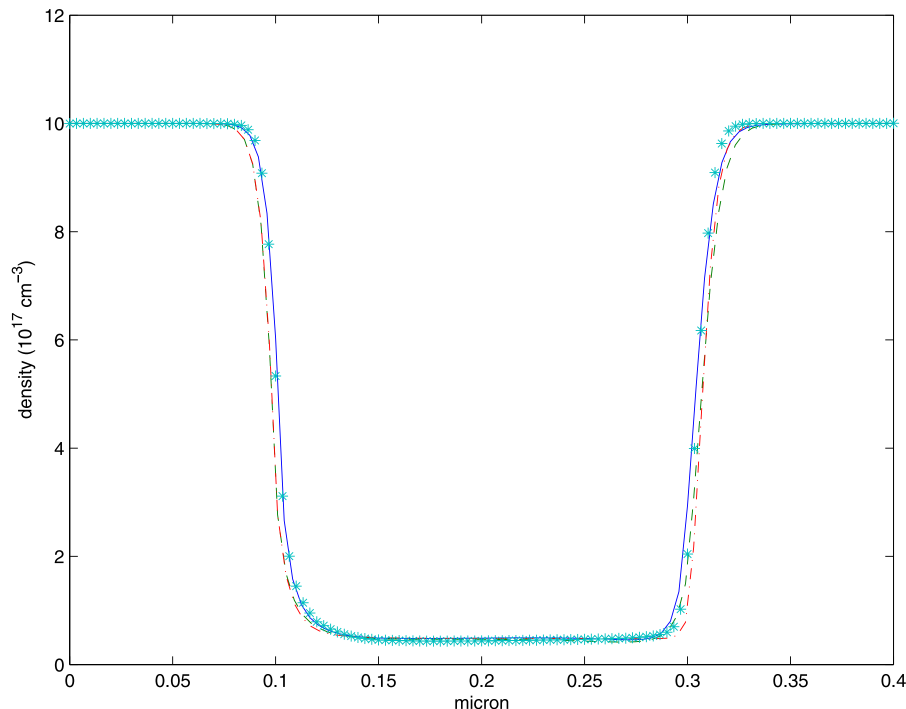

Fig. 2. Stationary solution for the density ($10^{17}\,\mathrm{cm}^{-3}$) in the diode with $L_C = 0.2\,\mu\mathrm{m}$. The stars are the Boltzmann solution, the continuous line is the MEP model, the dashed and dashed-dotted lines are the Stratton and drift-diffusion models respectively.

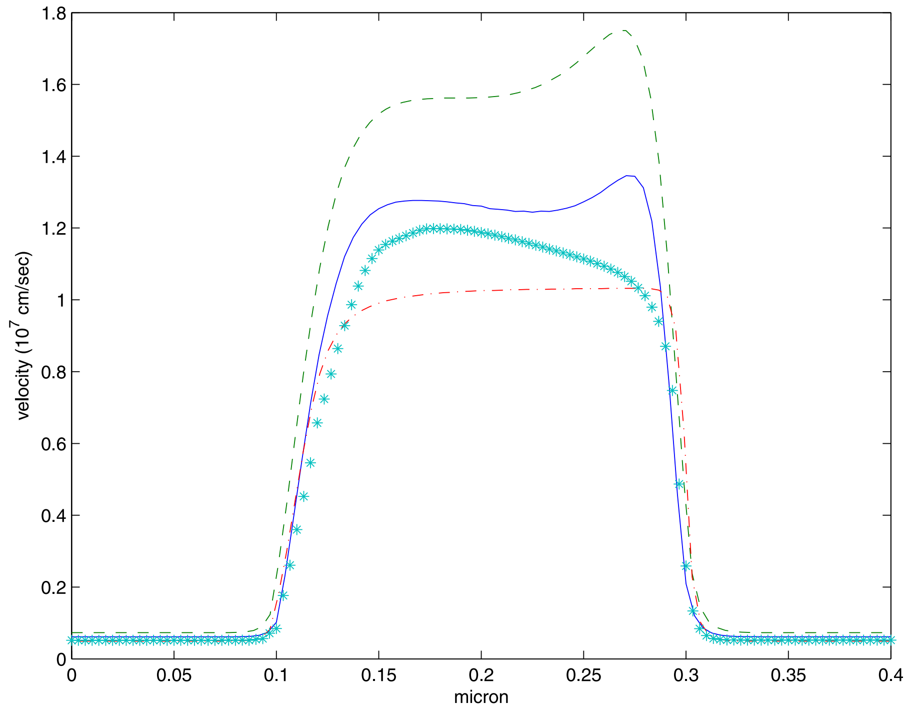

Fig. 3. Stationary solution for the electron velocity (10^7 cm/s) in the diode with $L_C = 0.2$ μm. The notation is as in Fig. 2.

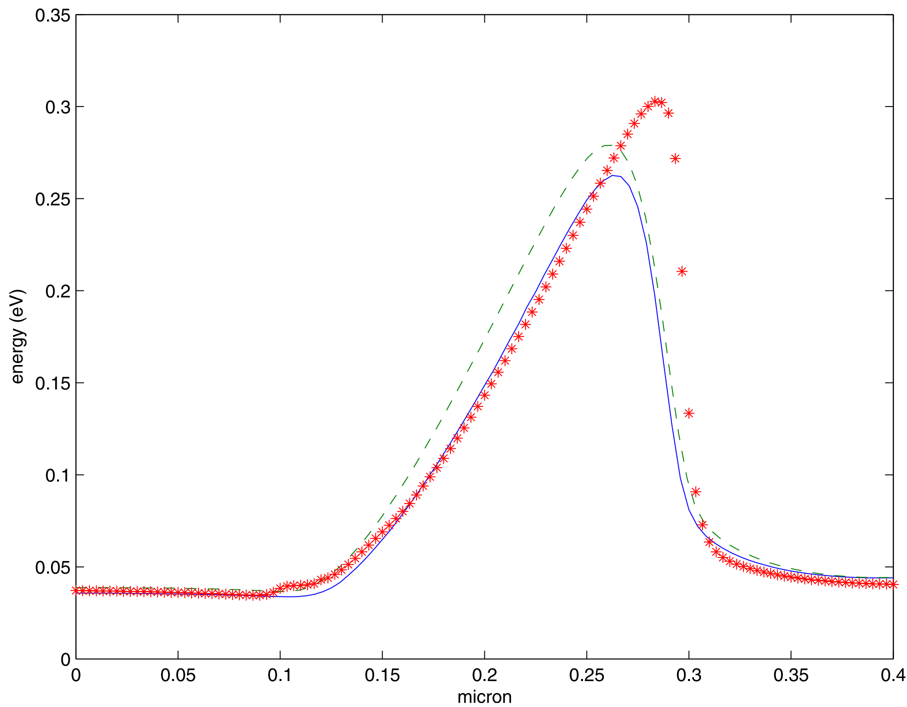

Fig. 4. Stationary solution for the electron energy (eV) in the diode with $L_C = 0.2$ μm. The notation is as in Fig. 2. The result with the drift-diffusion model is omitted because the energy is kept at equilibrium.

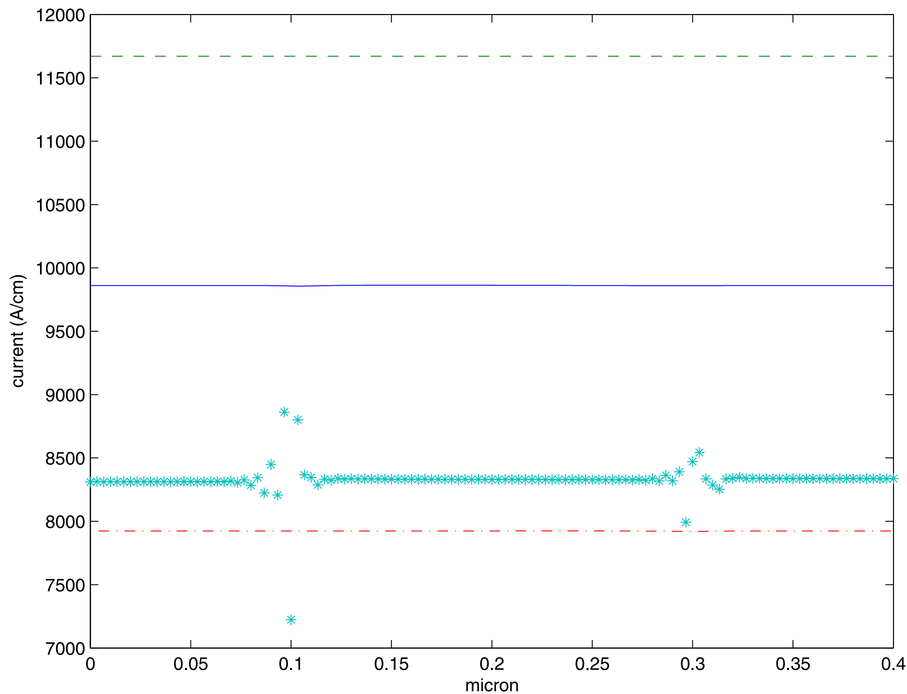

Fig. 5. Stationary solution for the current (A/cm^2) in the diode with $L_C = 0.2$ μm. The notation is as in Fig. 2.

In the sequel of this section only the grid with 96 points will be used because the results are already accurate enough. In particular the current is well conserved even across the junctions (see Fig. 5).

Concerning the validity of the model we have performed a comparison of the results obtained with the MEP and Stratton energy-transport model, the drift-diffusion model and a direct simulation of the Boltzmann transport equation [24]. The results are collected in the Figs. 2–16 for channel length of 0.05 and 0.025 μm.

The MEP model is more accurate than the Stratton one while the drift-diffusion model is not bad, although the energy is kept at the equilibrium value. The mean error of the Stratton model is roughly twice that of the MEP model.

The drift-diffusion is, apart the energy, still competitive, if one is not interested in thermal effects. It gives a poor description of velocity and density in the channel, especially in the shorter devices, but predicts values of currents with an error comparable with that present in the MEP model. Of course the use of the drift-diffusion for devices as MOSFETs, where it is crucial the electron dynamics in the channel, is very dubious.

5. Simulation of a 2D silicon MESFET

In this section we check the validity and efficiency of the numerical method by simulating a bidimensional metal semiconductor field effect transistor (MESFET) with the MEP model. Also in this case the other models are less accurate of the MEP one, as shown for example in [5].

The shape of the device is pictured in Fig. 17. The device has a 0.4 μm channel. The source and drain depths are 0.1 μm and the contact at the gate is 0.2 μm. The distance between the gate and the other two contacts is 0.1 μm. The lateral subdiffusion of the source and the drain region is about 0.05 μm. The same doping concentration as in [29] is considered

$$n_D(x) - n_A(x) = \begin{cases} n_+ = 3 \times 10^{17}\ \text{cm}^{-3} & \text{in the n}^+ \text{ regions,} \\ n_- = 10^{17}\ \text{cm}^{-3} & \text{in the n region} \end{cases}$$

with abrupt junctions.

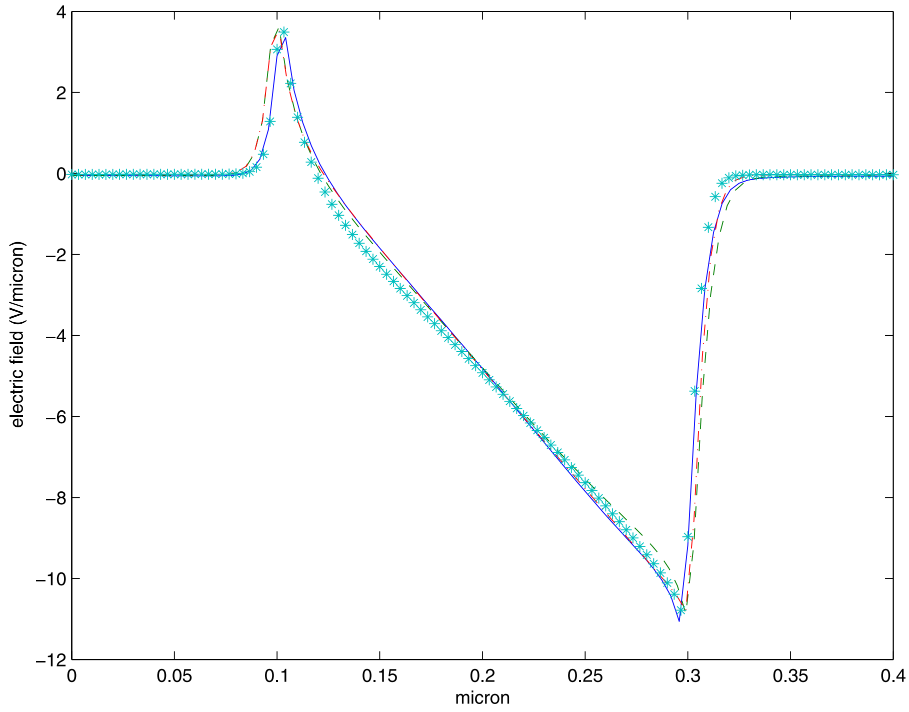

Fig. 6. Stationary solution for the electric field (V/μm) in the diode with $L_C = 0.2$ μm. The notation is as in Fig. 2.

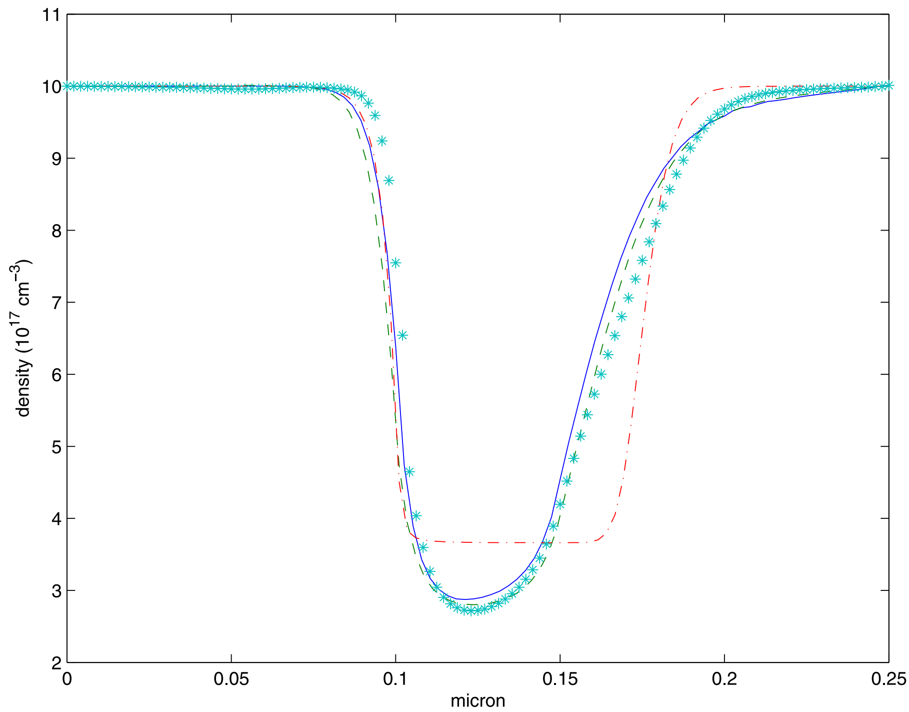

Fig. 7. Stationary solution for the density (10^{17} cm^{-3}) in the diode with $L_C = 0.05$ μm. The notation is as in Fig. 2.

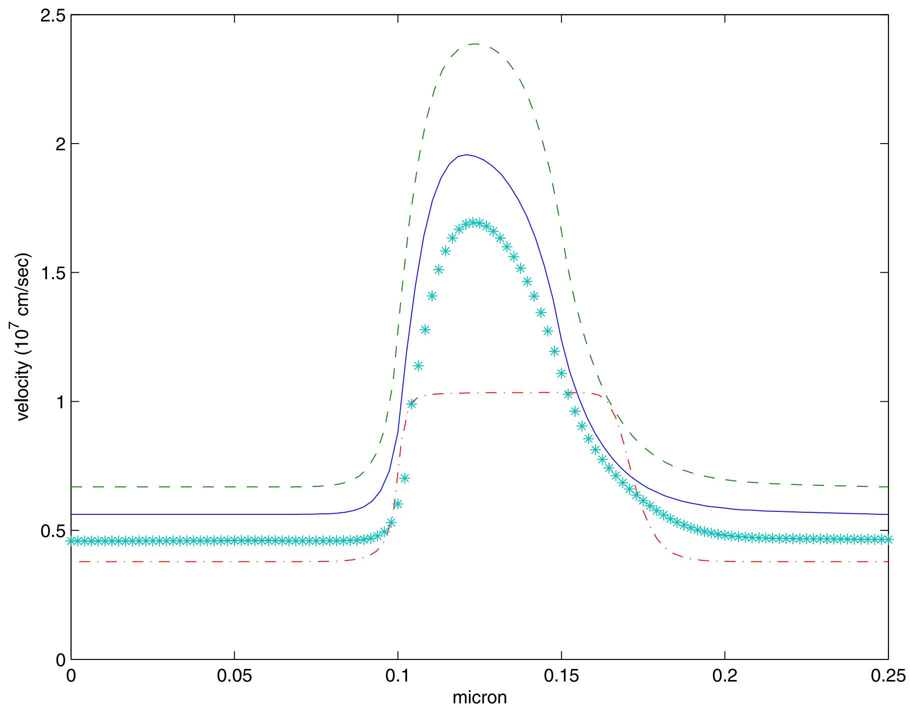

Fig. 8. Stationary solution for the electron velocity (10^7 cm/s) in the diode with $L_C = 0.05$ μm. The notation is as in Fig. 2.

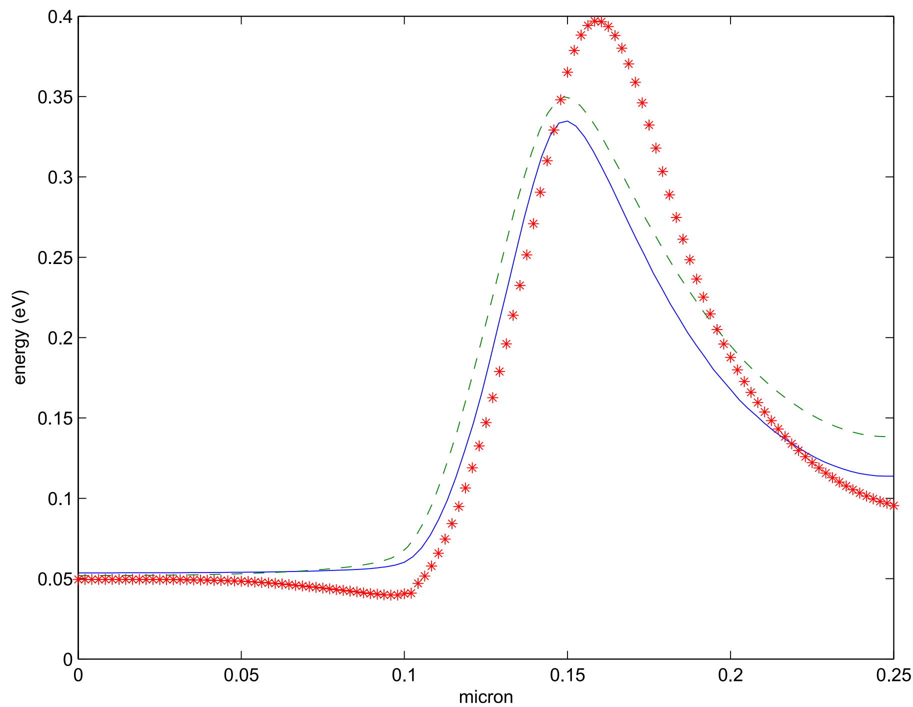

Fig. 9. Stationary solution for the electron energy (eV) in the diode with $L_C = 0.05$ μm. The notation is as in Fig. 2. The result with the drift-diffusion model is omitted because the energy is kept at equilibrium.

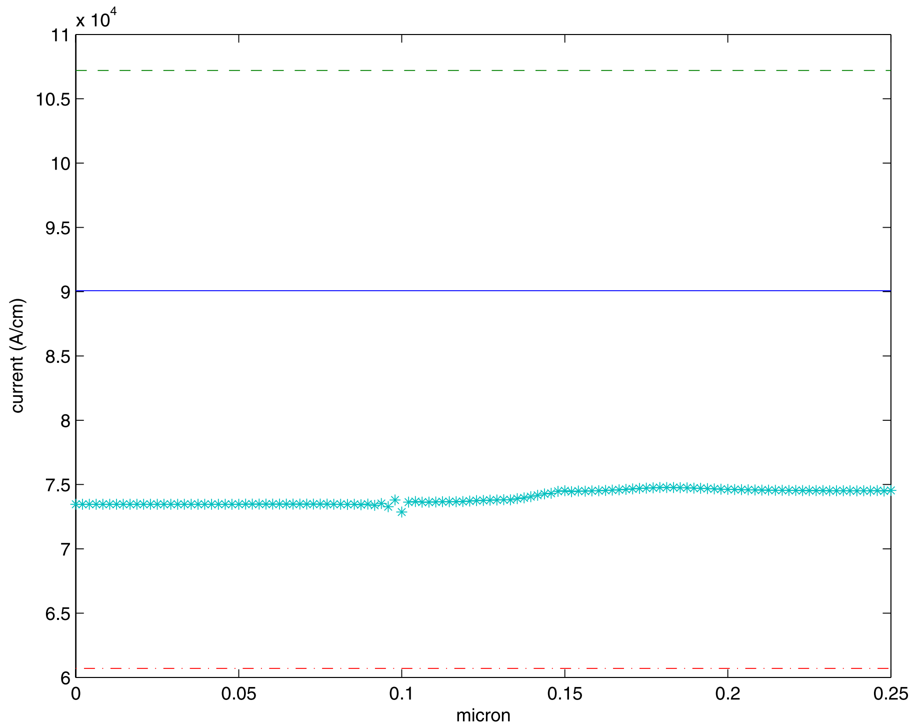

Fig. 10. Stationary solution for the current (A/cm^2) in the diode with $L_C = 0.05$ μm. The notation is as in Fig. 2.

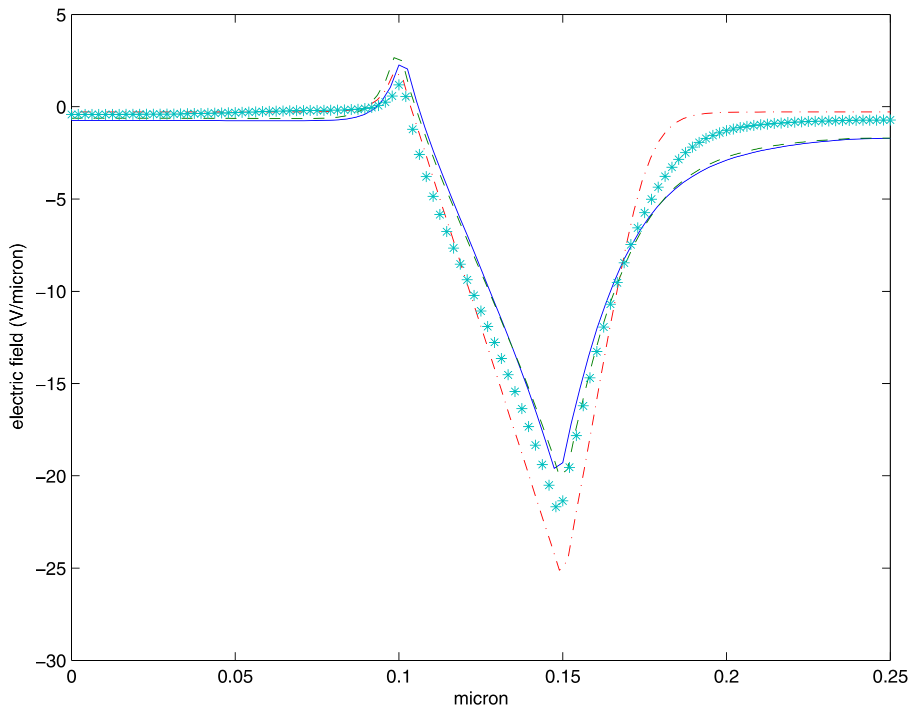

Fig. 11. Stationary solution for the electric field (V/μm) in the diode with $L_C = 0.05$ μm. The notation is as in Fig. 2.

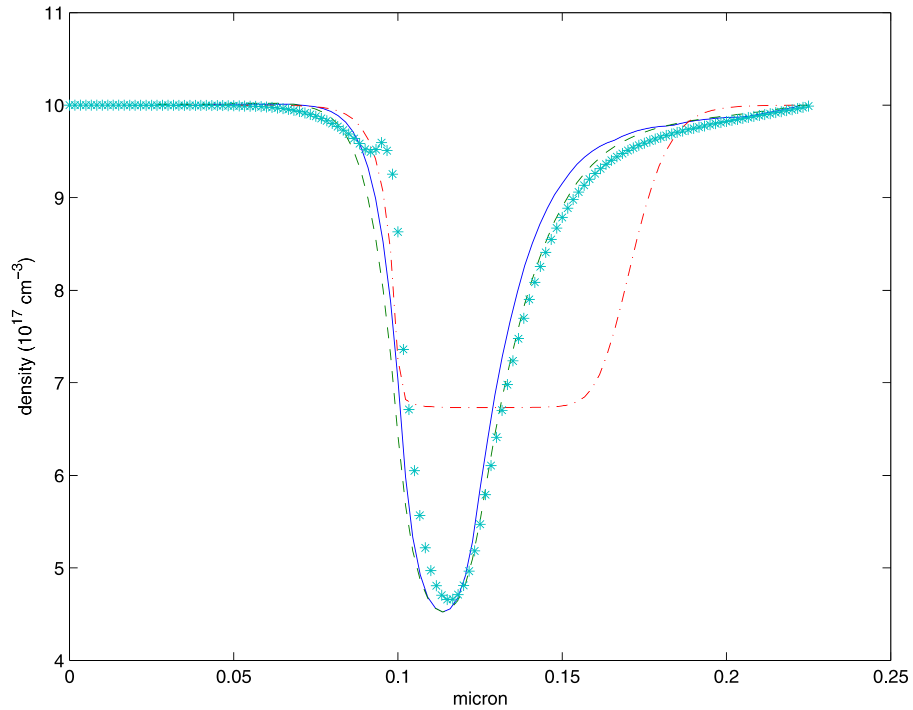

Fig. 12. Stationary solution for the density (10^{17} cm^{-3}) in the diode with $L_C = 0.025$ μm. The notation is as in Fig. 2.

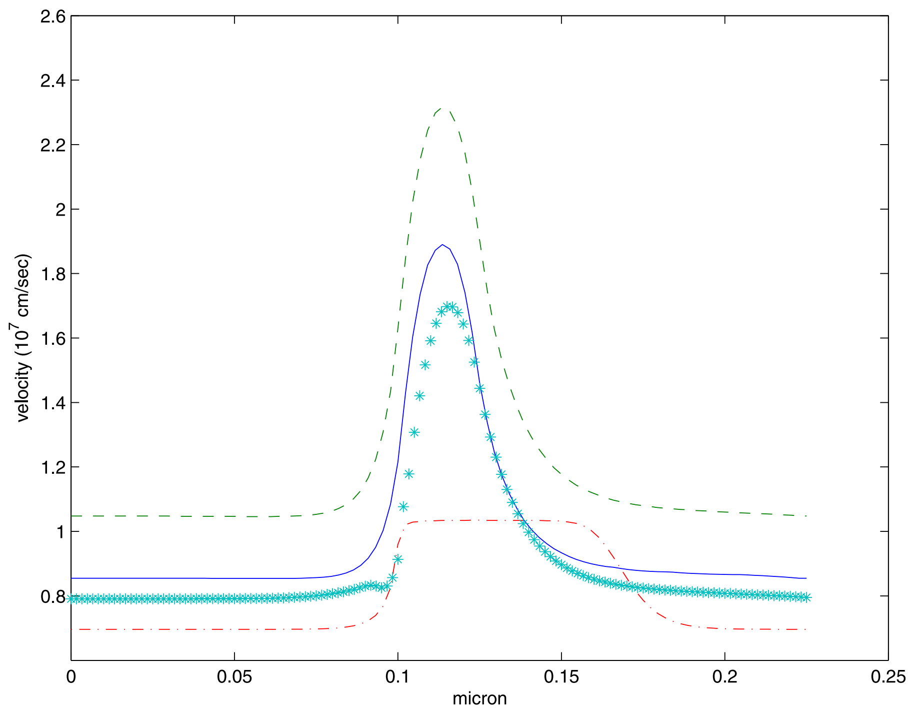

Fig. 13. Stationary solution for the electron velocity (10^7 cm/s) in the diode with $L_C = 0.025$ μm. The notation is as in Fig. 2.

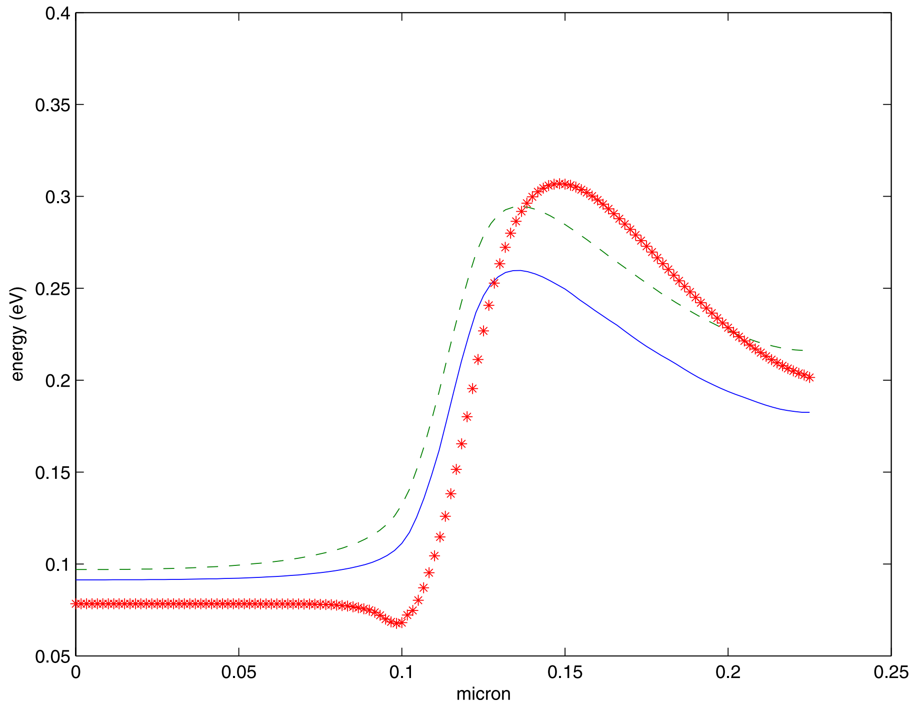

Fig. 14. Stationary solution for the electron energy (eV) in the diode with $L_C = 0.025$ μm. The notation is as in Fig. 2. The results with the drift-diffusion model are omitted.

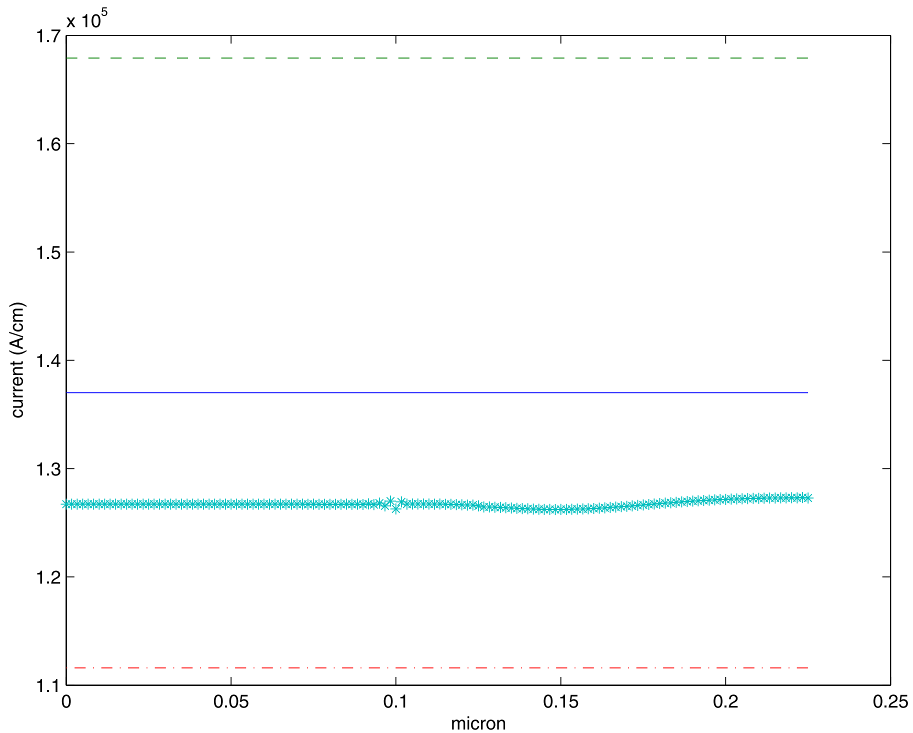

Fig. 15. Stationary solution for the current (A/cm^2) in the diode with $L_C = 0.025$ μm. The notation is as in Fig. 2.

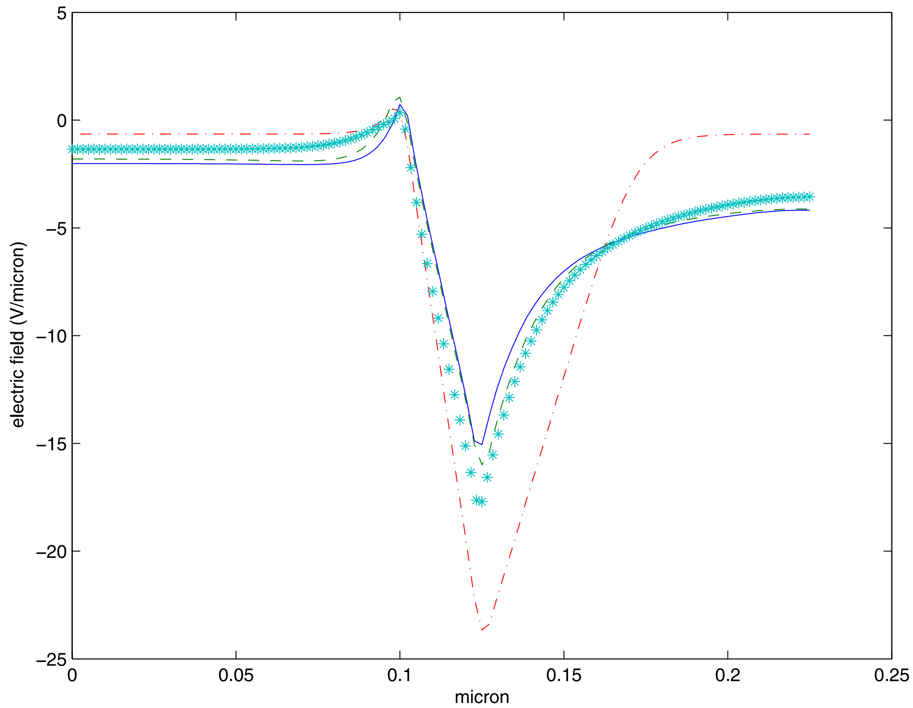

Fig. 16. Stationary solution for the electric field (V/μm) in the diode with $L_C = 0.025$ μm. The notation is as in Fig. 2.

We take a reference frame with axes parallel to the edges of the device. The numerical domain representing the MESFET is

$$\Omega = [0, 0.6] \times [0, 0.2],$$

where the unit length is in μm.

The regions of high doping n^+ are the subset

$$[0, 0.1] \times [0.15, 0.2] \cup [0.5, 0.6] \times [0.15, 0.2].$$

We denote by Γ_D that part of $\partial\Omega$, the boundary of Ω, which represents the source, gate and drain

$$\Gamma_D = \{(x, y) : y = 0.2, 0 \leqslant x \leqslant 0.1, 0.2 \leqslant x \leqslant 0.4, 0.5 \leqslant x \leqslant 0.6\}.$$

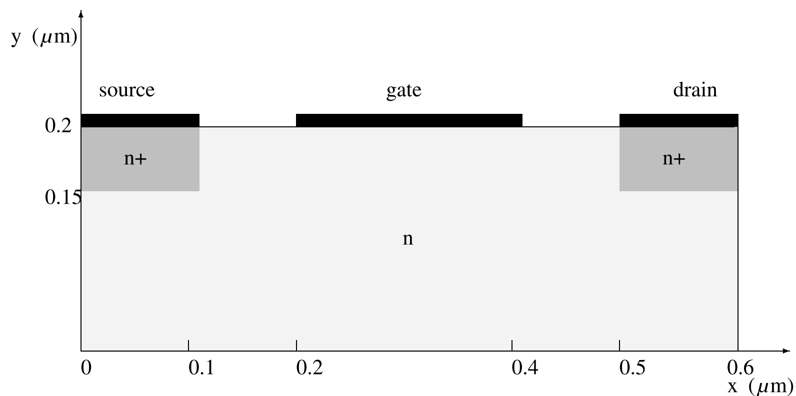

Fig. 17. Schematic representation of a bidimensional MESFET.

The other part of $\partial\Omega$ is labelled as Γ_N. The boundary conditions are assigned as follows. We have ohmic contacts at source and drain:

$$n = n_+, \quad W = \frac{3}{2} k_B T_L, \quad \Phi = \begin{cases} \Phi_b & \text{at drain,} \\ 0 & \text{at source.} \end{cases} \tag{49}$$

On the gate we have a Schottky contact

$$n = n_g, \quad W = \frac{3}{2} k_B T_L, \quad \Phi = \Phi_g. \tag{50}$$

Indeed the potential at the contacts should include the built-in potential and the density at the gate should be related to the potential. Here we do not enter into the details of the modelling of the Schottky contacts (see for example [30]) and, by using the invariance of the electric field with respect to change of the potential with respect additive constants, set

$$n_g = 3.9 \times 10^5 \text{ cm}^{-3}, \quad \Phi_g = -0.8 \text{ V}.$$

In the remaining part Γ_N of the boundary we have

$$\boldsymbol{v} \cdot \nabla n = 0, \quad \boldsymbol{v} \cdot \nabla W = 0, \quad \boldsymbol{v} \cdot \nabla \phi = 0, \quad i = 1, 2. \tag{51}$$

Here ∇ is the bidimensional gradient operator while $\boldsymbol{v}$ is the unit outward normal vector to $\partial\Omega$ in the con... ered points.

We remark that the boundary conditions for the MEP energy-transport model are more clear th... ogous ones for the full hydrodynamical model wherefrom it is derived (see [22]).

Two cases are considered: $\Phi_b = 1.5$ V and $\Phi_b = 2$ V. In both situations the stationar... after about 5 ps.

The stationary value of density, energy, components of the electric field and ... 18–22. There is the typical depletion region close to the gate with the pres... numerically well described.

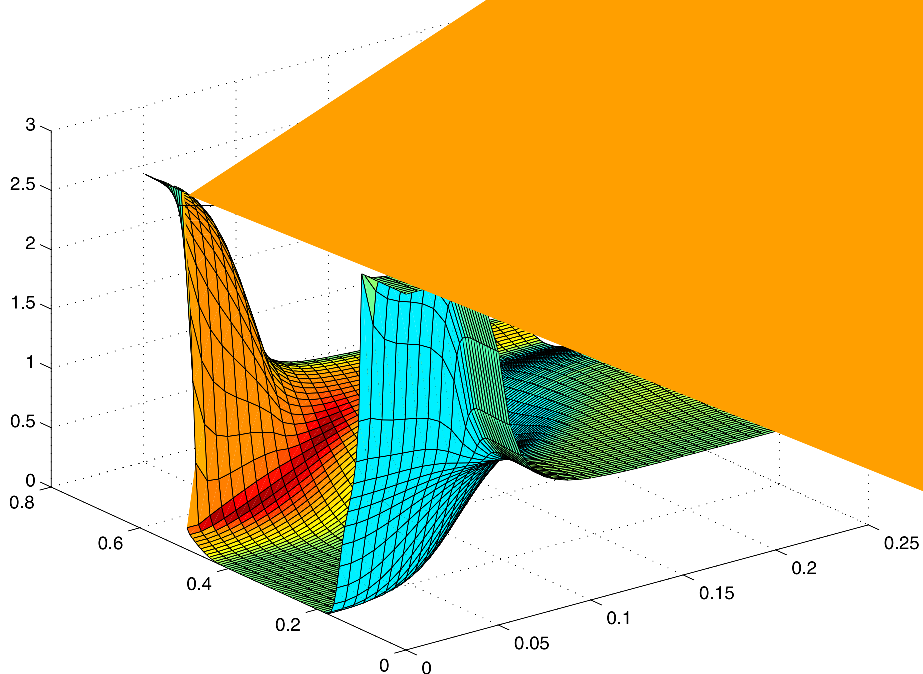

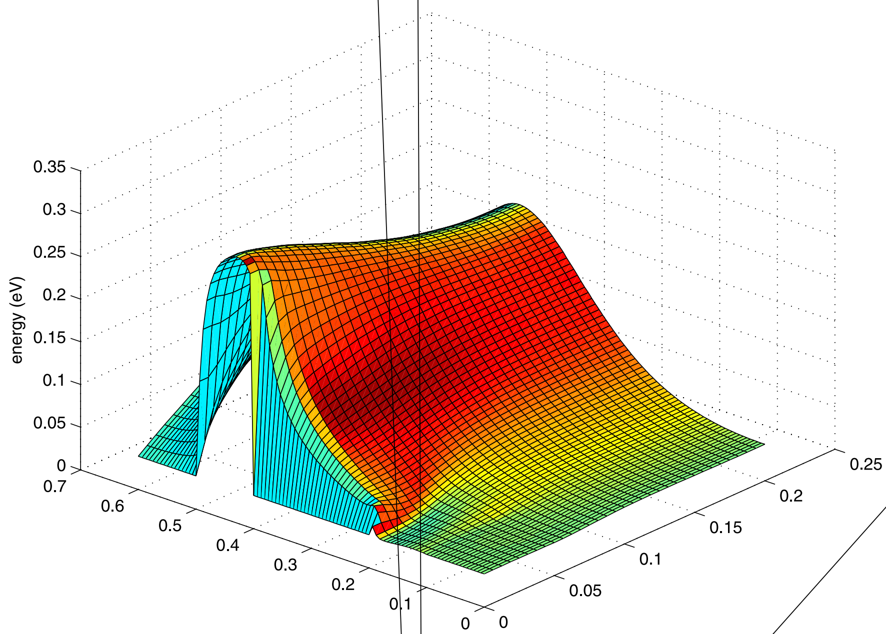

Fig. 19. Stationary solution for the electron energy (eV) in MESFET for $\Phi_b = 2$ V.

On account of the mixed boundary conditions, the solution has a loss of regularity at the edges of drain and source according to [31]. The scheme developed in the previous section furnishes the component of the current along the direction orthogonal to the contacts in the middle points of the grid as shown in Fig. 1. By taking into account that the longitudinal component of **J** is zero at contacts as consequence of the boundary conditions, a simple approximation of the significant component of the current at the contacts can be obtained with

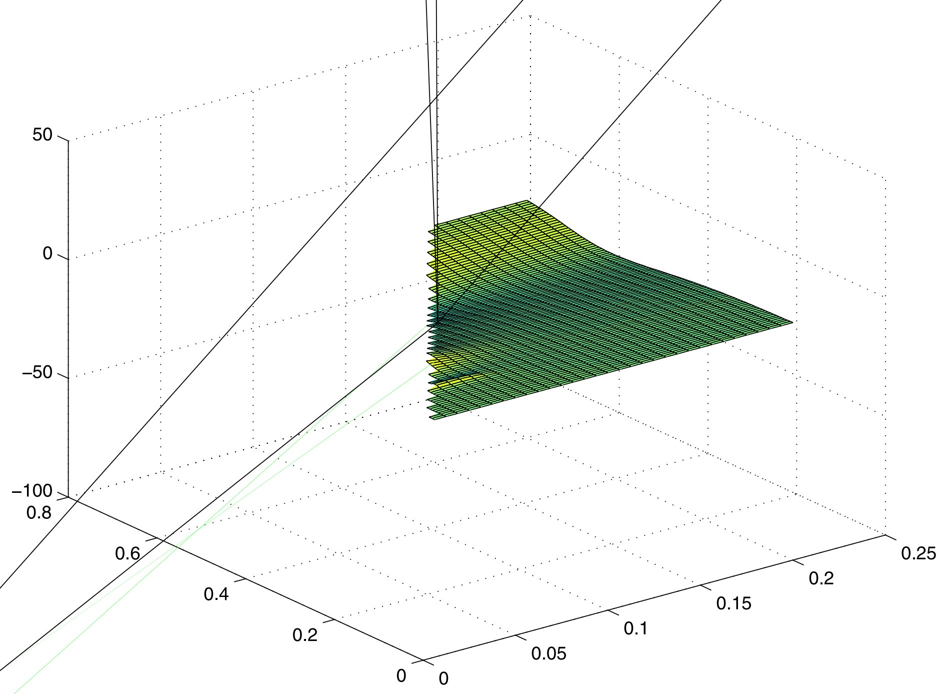

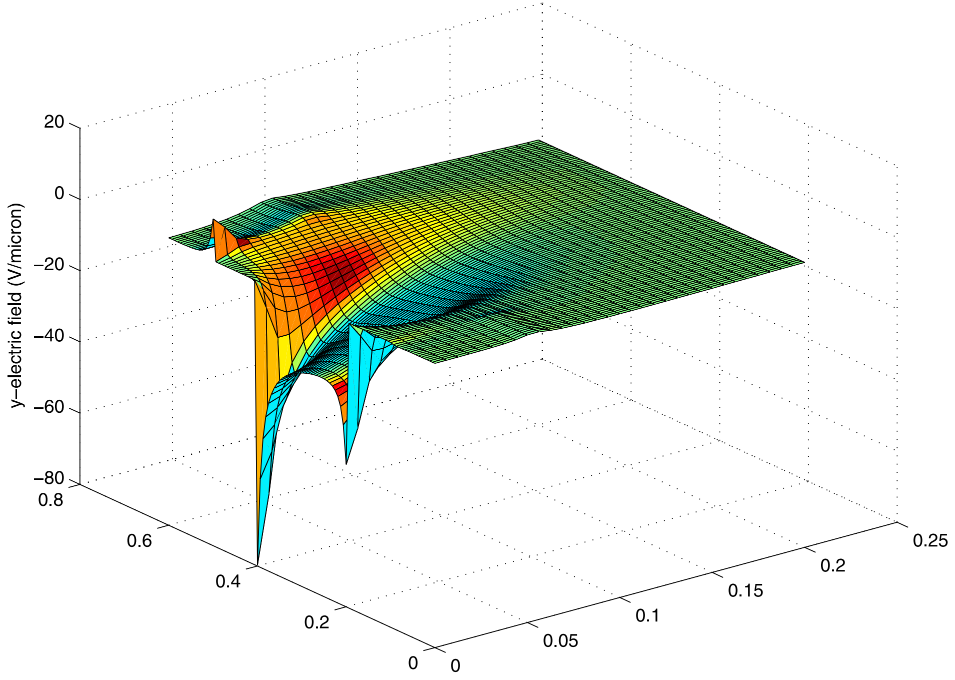

Fig. 21. Stationary solution for the y-component of the electric field (V/μm) in MESFET for $\Phi_b = 2$ V.

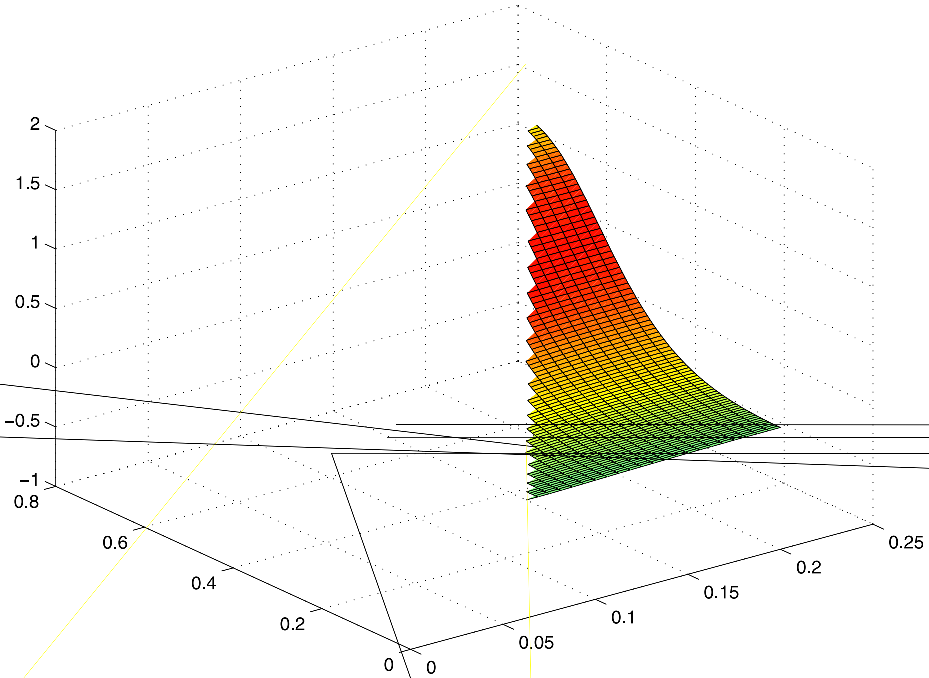

$$J^{(r)}_{i,j_c} = -\frac{(g_{1r})_{i,j_c+1} - (g_{1r})_{i,j_c}}{k} + q\bar{\lambda}^W (g_{1r})_{i,j_c} \frac{\phi_{i,j_c+1} - \phi_{i,j_c}}{k} + \mathrm{O}(k), \quad r = 1, 2, \tag{52}$$

where we have denoted with (i, j_c), $i = i_a, \ldots, i_b$, the indexes of the grid points at the contacts.

Table 2
Absolute value of current (A/μm) at source (I_s), gate (I_g) and drain (I_d) for some values of Φ_b and Φ_g

Φ_b (V)	Φ_g (V)	I_s	I_g	I_d
1.5	−.8000	−1.573	.03009	1.586
2.0	−.8000	−1.677	.0091	1.680

The loss of regularity of the solution produces a considerable difference between the absolute value of the current at drain and source. To overcome this problem we approximate the currents at the contacts through their values at the middle points

$$J^{(r)}_{i,j_c} = J^{(r)}_{i,j_c+1/2} + \mathrm{O}(k), \quad r = 1,2 \tag{53}$$

operating a sort of numerical regularization from the interior. The error is of the order of the mesh size as in (52) but the problem related to the presence of huge gradients is avoided. With this approach a good charge conservation is obtained, as shown by the results of Table 2.

6. Simulation of a 2D silicon MOSFET

In this section we check the validity and efficiency of the numerical method by simulating a bidimensional metal oxide semiconductor field effect transistor (MOSFET). The shape of the device is pictured in Fig. 23.

The device has a 0.2 μm channel. The source and drain depths are 0.1 μm and the contact at the gate is 0.15 μm. The distance between the gate and the other two contacts is 0.025 μm. The lateral subdiffusion of the source and the drain region is about 0.05 μm. The gate oxide is 0.15 μm long and 20 nm thick.

The doping concentration is

$$n_D(x) - n_A(x) = \begin{cases} n_+ = 10^{17}\ \mathrm{cm}^{-3} & \text{in the n}^+ \text{ regions,} \\ -p_- = -10^{14}\ \mathrm{cm}^{-3} & \text{in the p region} \end{cases}$$

with abrupt junctions.

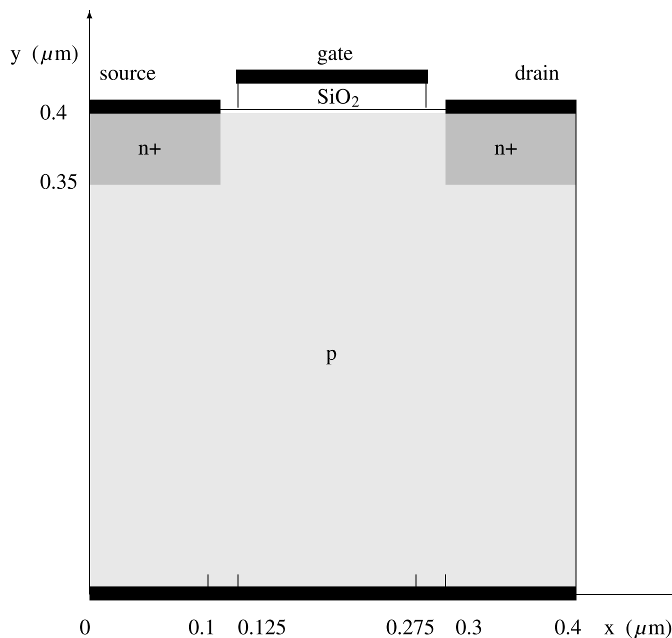

Fig. 23. Schematic representation of a bidimensional MOSFET.

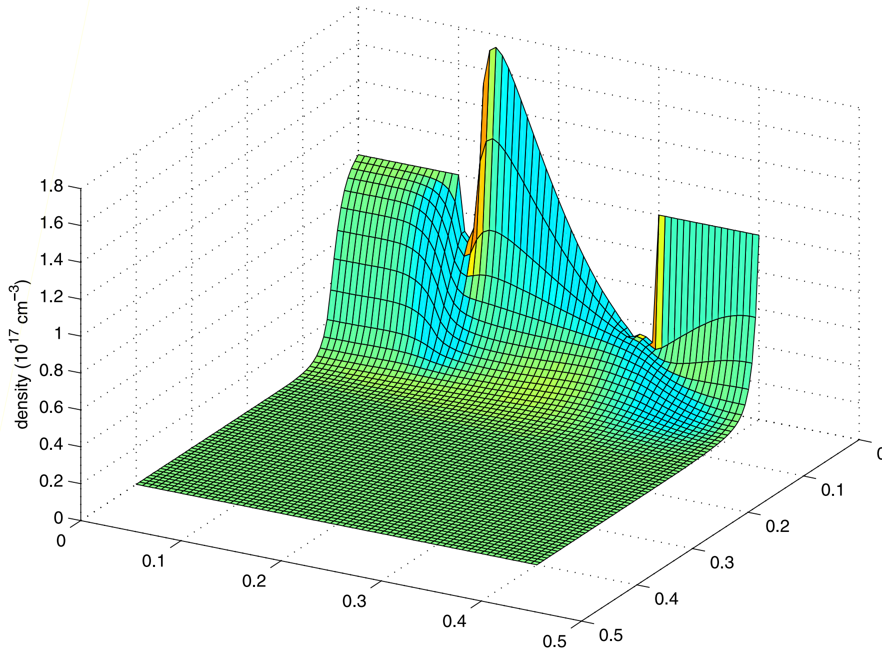

Fig. 24. Stationary solution for the electron density in MOSFET (10^{17} cm^{-3}) for $V_{DS} = 1$ V and $V_{DG} = 0.8$ V.

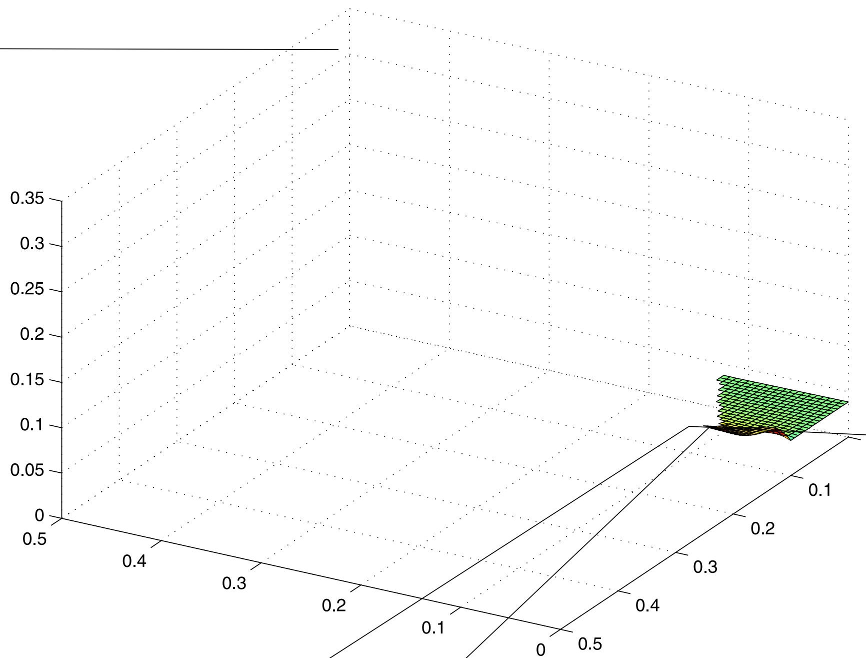

Fig. 25. Stationary solution for the electron energy in MOSFET (eV) for $V_{DS} = 1$ V and $V_{DG} = 0.8$ V.

At variance with MESFET, there are different built-in potentials we explicitly take into account by using the simple model

$$\Phi_b^D = \Phi_b^S = \frac{k_B T_L}{e} \ln \frac{n_+}{n_i}$$

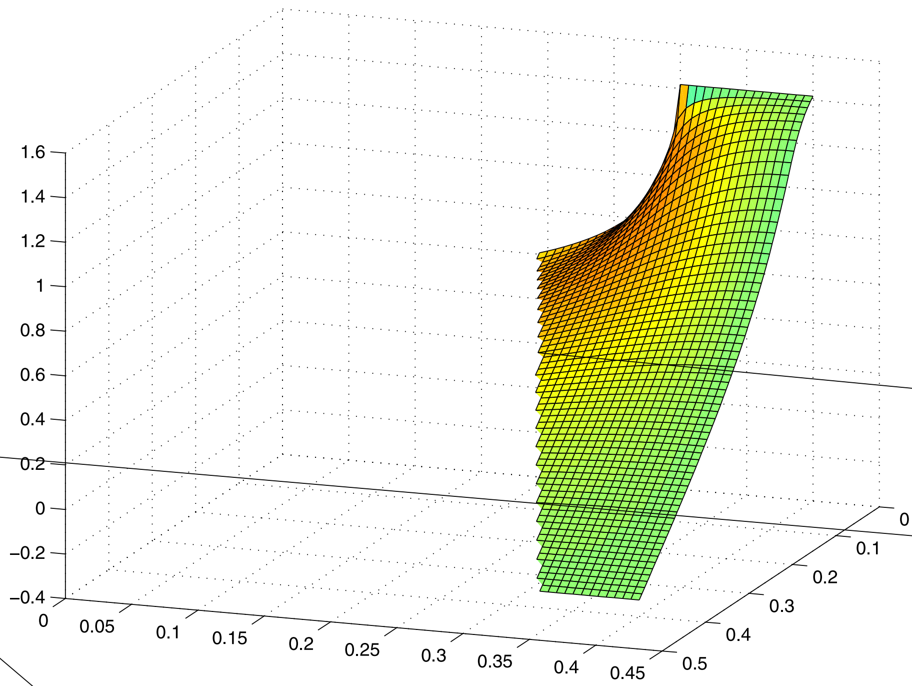

at drain and source,

$$\Phi_{\mathrm{b}}^{B} = -\frac{k_{\mathrm{B}} T_{\mathrm{L}}}{e} \ln \frac{p_{-}}{n_{\mathrm{i}}}$$

at bulk contact. n_{i} is the intrinsic electron concentration ($10^{10}\ \mathrm{cm}^{-3}$).

If the reference axes are chosen parallel to the edges of the device. The silicon part of the MOSFET is represented by the numerical domain

$$[0, 0.4] \times [0, 0.4]$$

and at the top of the silicon part the silicon oxide domain is

$$[0.125, 0.275] \times [0.4, 0.42],$$

where the length is in μm.

The regions of high-doping n^+ are the subset

$$[0, 0.1] \times [0.35, 0.4] \cup [0.3, 0.4] \times [0.35, 0.4].$$

A uniform mesh of 64×64 grid points has been used.

We have assumed ohmic contacts on the source, drain, gate and bulk base contacts, homogeneous Neumann conditions on the remaining part of the boundary. The surface charge at the oxide interface is neglected and the continuity of the electric potential and electric field is imposed. The values of density and energy at the interface are obtained by the interior grid points with a linear interpolation in the direction orthogonal to the boundary.

In order to reach the desired bias, we have needed to resort to a continuation method on applied potential. First, we iterate with respect to the difference of the built-in potential between drain and bulk contacts, keeping at zero V_{DS}. Then we iterate with respect to the drain–gate potential and finally we increase the drain–source potential.

The 2D solution of the MEP model is plotted in Figs. 24–28 for $V_{DS} = 1$ V and $V_{DG} = 0.8$ V. All the main features of the electron dynamics are well described, in particular the charge accumulation beside the oxide and the pronounced depletion at the drain contact due to the strong electric field (a similar result was been obtained in [5], Fig. 26). We note an effect of heating in the bulk.

Again the density current presents a singularity at the first edge of drain and therefore we evaluated the current by considering, as for MESFET, the regularization from the interior (see Fig. 29). The characteristic curves for several V_{DG} are shown in Fig. 30.

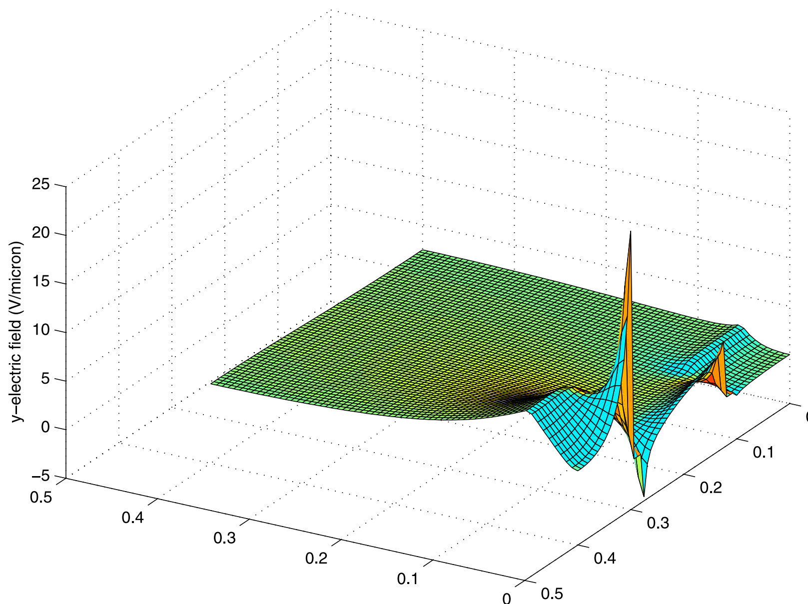

Fig. 28. Stationary solution for the y-component of the electric field in MOSFET (V/μm) for $V_{DS} = 1$ V and $V_{DG} = 0.8$ V.

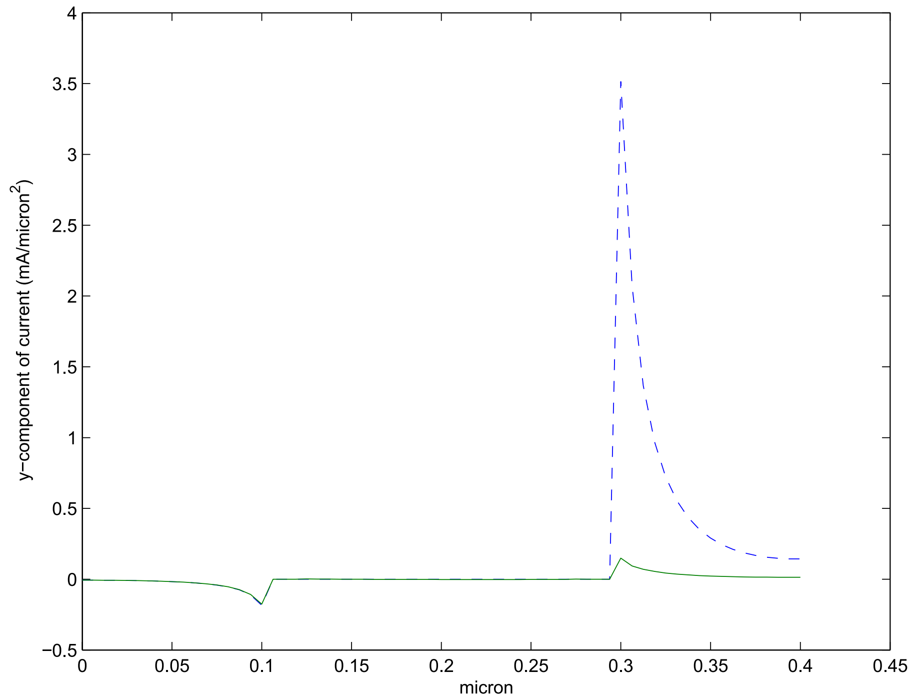

Fig. 29. y-Component of the density current (mA/μm^2) at $y = 0.4$ μm. The dashed line is the density current given by (52), the continuous line is the regularization from the interior given by (53). Note the singularity at the source for $x = 0.3$ μm.

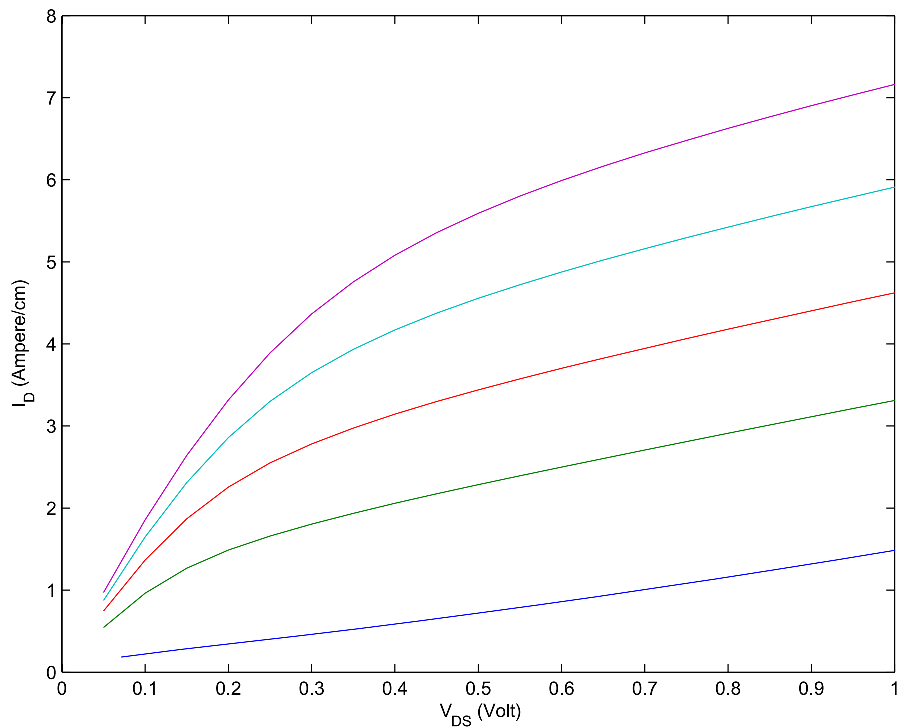

Fig. 30. Drain current I_D (A/cm) for $V_{DG} = 0.5, 0.8, 1, 1.2, 1.4$ V. The current increases as V_{DG} increases.

7. Conclusions and Acknowledgments

The MEP energy-transport model for charge transport in semiconductor used in this article is free of any fitting parameters and is based on sound and consistent physical principles. A suitable numerical finite difference scheme has been formulated. Simulations of silicon diodes, MESFETs and MOSFETs show that it is very robust and guarantees accurate current conservation.

The author is indebted to Prof. A. Majorana for providing the results of the direct simulations of the transport Boltzmann equation.

The author acknowledges the financial support by M.I.U.R. (PRIN 2004 *Problemi Matematici delle teorie cinetiche*), P.R.A. University of Catania (ex 60%), CNR (Grant No. 00.00128.ST74), the EU Marie Curie RTN Project COMSON Grant No. MRTN-CT-2005-019417.

Appendix A. Summary of the closure relations

In Table 3 we report the values of the physical parameters used in the simulations. Moreover for the sake of completeness we summarize all the functions entering in the constitutive equations (5) and (6). For more details, see [2–4].

Concerning the quantities U, F and G, one has

$$U = \frac{2}{3d_0}\int_0^\infty [\mathscr{E}(1+\alpha\mathscr{E})]^{3/2}\exp(-\lambda^W\mathscr{E})\,\mathrm{d}\mathscr{E}, \tag{54}$$

$$F = \frac{2}{3m^* d_0}\int_0^\infty \exp(-\lambda^W\mathscr{E})\frac{\mathscr{E}[\mathscr{E}(1+\alpha\mathscr{E})]^{3/2}}{1+2\alpha\mathscr{E}}\,\mathrm{d}\mathscr{E}, \tag{55}$$

$$G = \frac{1}{m^* d_0}\int_0^\infty \exp(-\lambda^W\mathscr{E})\left[1+\frac{2(1+\alpha\mathscr{E})}{3(1+2\alpha\mathscr{E})^2}\right]\mathscr{E}^{3/2}\sqrt{1+\alpha\mathscr{E}}\,\mathrm{d}\mathscr{E}. \tag{56}$$

where $\lambda^W(W)$ is the expression of the Lagrangian multipliers relative to the energy. It depends only on W and it is obtained by inverting the relation

$$W = \frac{\int_0^\infty \mathscr{E}\sqrt{\mathscr{E}(1+\alpha\mathscr{E})}(1+2\alpha\mathscr{E})\exp(-\lambda^W\mathscr{E})\,\mathrm{d}\mathscr{E}}{\int_0^\infty \sqrt{\mathscr{E}(1+\alpha\mathscr{E})}(1+2\alpha\mathscr{E})\exp(-\lambda^W\mathscr{E})\,\mathrm{d}\mathscr{E}}.$$

Note that U, F and G depend only on W as consequence of the fact that λ^W is function of W alone.

The production terms are the sum of the term due to the elastic scatterings (acoustic phonon scattering) and that due to inelastic phonon scatterings. Therefore the production matrix $\mathbf{C} = (c_{ij})$ is given by the sum $\mathbf{C} = \mathbf{C}^{(\mathrm{ac})} + \mathbf{C}^{(\mathrm{np})}$.

Concerning the acoustic phonon scattering, the contribution to the energy balance equation is zero while the production matrix $\mathbf{C}^{(\mathrm{ac})} = (c_{ij}^{(\mathrm{ac})})$ can be written as $\mathbf{C}^{(\mathrm{ac})} = \mathbf{A}^{(\mathrm{ac})}\mathbf{B}$. The coefficients b_{ij} of the matrix $\mathbf{B}$ are given by

Table 3
Values of the physical parameters

m_e (g)	Electron rest mass	9.1095×10^{-28}
m^*	Effective electron mass	$0.32m_e$
T_L (K)	Lattice temperature	300
ρ (g/cm^3)	Density	2.33
v_s (cm/s)	Longitudinal sound speed	9.18×10^5
Ξ_d (eV)	Acoustic-phonon deformation potential	9
α (eV^{-1})	Non-parabolicity factor	0.5
ϵ_r	Si relative dielectric constant	11.7
ϵ_{ro}	SiO_2 relative dielectric constant	3.9
ϵ_0 (C/V μm)	Vacuum dielectric constant	8.85×10^{-18}

$$b_{11} = \frac{a_{22}}{\Delta}, \quad b_{12} = -\frac{a_{12}}{\Delta}, \quad b_{22} = \frac{a_{11}}{\Delta}$$

with

$$a_{11} = -\frac{2p_0}{3m^* d_0}, \quad a_{12} = -\frac{2p_1}{3m^* d_0}, \quad a_{22} = -\frac{2p_2}{3m^* d_0}, \quad \Delta = a_{11}a_{22} - a_{12}^2,$$

$$d_k = \int_0^\infty \mathscr{E}^k \sqrt{\mathscr{E}(1+\alpha\mathscr{E})}(1+2\alpha\mathscr{E}) \exp(-\lambda^{W(0)}\mathscr{E})\, d\mathscr{E}, \quad k = 0, 1, \ldots$$

$$p_k = \int_0^\infty \frac{[\mathscr{E}(1+\alpha\mathscr{E})]^{3/2}\mathscr{E}^k}{1+2\alpha\mathscr{E}} \exp(-\lambda^{W(0)}\mathscr{E})\, d\mathscr{E}, \quad k = 0, 1, \ldots .$$

The coefficients of the matrix $\mathbf{A}^{(\mathrm{ac})}$ read

$$a_{11}^{(\mathrm{ac})} = \frac{\overline{K}_{\mathrm{ac}}}{d_0} \int_0^\infty \mathscr{E}^2 (1+\alpha\mathscr{E})^2 (1+2\alpha\mathscr{E}) \exp(-\lambda^W \mathscr{E})\, d\mathscr{E}, \tag{57}$$

$$a_{12}^{(\mathrm{ac})} = \frac{\overline{K}_{\mathrm{ac}}}{d_0} \int_0^\infty \mathscr{E}^3 (1+\alpha\mathscr{E})^2 (1+2\alpha\mathscr{E}) \exp(-\lambda^W \mathscr{E})\, d\mathscr{E}, \tag{58}$$

$$a_{21}^{(\mathrm{ac})} = \frac{\overline{K}_{\mathrm{ac}}}{m^* d_0} \int_0^\infty \mathscr{E}^3 (1+\alpha\mathscr{E})^2 \exp(-\lambda^W \mathscr{E})\, d\mathscr{E}, \tag{59}$$

$$a_{22}^{(\mathrm{ac})} = \frac{\overline{K}_{\mathrm{ac}}}{m^* d_0} \int_0^\infty \mathscr{E}^4 (1+\alpha\mathscr{E})^2 \exp(-\lambda^W \mathscr{E})\, d\mathscr{E}, \tag{60}$$

where

$$\overline{K}_{\mathrm{ac}} = \frac{8\pi\sqrt{2}(m^*)^{3/2} K_{\mathrm{ac}}}{3\hbar^3}, \quad K_{\mathrm{ac}} = \frac{k_{\mathrm{B}} T_{\mathrm{L}} \Xi_d^2}{4\pi^2 \hbar \rho v_{\mathrm{s}}^2}.$$

Concerning the non-polar phonon scattering the production term of the energy balance equation is given by $C_W = \sum_{A=1}^{6} C_{W_A}$, where for each valley

$$C_{W_A} = \frac{3}{2} \frac{\overline{K}_{\mathrm{np}}}{d_0} \sum_{\pm} \left(n_{\mathrm{B}} + \frac{1}{2} \mp \frac{1}{2}\right) \left[\exp\left(\pm \frac{\hbar\omega_{\mathrm{np}}}{k_{\mathrm{B}} T_{\mathrm{L}}} \mp \lambda^W \hbar\omega_{\mathrm{np}}\right) - 1\right] \eta^{\pm} \tag{61}$$

with

$$\eta^{\pm} = \int_{\hbar\omega_{\mathrm{np}} H(1\mp 1)}^{\infty} \mathscr{E} \mathscr{N}_{\pm} \sqrt{\mathscr{E}(1+\alpha\mathscr{E})}(1+2\alpha\mathscr{E}) \exp(-\lambda^{W\mathscr{E}})\, d\mathscr{E}, \tag{62}$$

$$\mathscr{N}_{\pm} = \sqrt{(\mathscr{E} \pm \hbar\omega_{\mathrm{np}})[1+\alpha(\mathscr{E} \pm \hbar\omega_{\mathrm{np}})]}[1+2\alpha(\mathscr{E} \pm \hbar\omega_{\mathrm{np}})] \tag{63}$$

and

$$\overline{K}_{\mathrm{np}} = \frac{8\pi\sqrt{2}(m^*)^{3/2} K_{\mathrm{np}}}{3\hbar^3}, \quad K_{\mathrm{np}} = Z_{\mathrm{f}} \frac{(D_t K)^2}{8\pi^2 \rho \omega_{\mathrm{np}}}.$$

H is the Heaviside function

$$H(x) = \begin{cases} 1 & \text{if } x > 0, \\ 0 & \text{otherwise.} \end{cases}$$

The coefficients of the production matrix $\mathbf{C}^{(\mathrm{np})} = (c_{ij}^{(\mathrm{np})})$ are given by $c_{ij}^{(\mathrm{np})} = \sum_{A=1}^{6} c_{A_{ij}}^{(\mathrm{np})}$. For each valley one has $\mathbf{C}^{(\mathrm{np})} = \mathbf{A}^{(\mathrm{np})} B$, where the matrix $\mathbf{A}^{(\mathrm{np})}$ has components

$$a_{11}^{(\mathrm{np})} = \frac{\overline{K}_{\mathrm{np}}}{d_0} \sum_{\pm} \left(n_B + \frac{1}{2} \mp \frac{1}{2}\right) \int_{\hbar\omega_{\mathrm{np}} H(1\mp 1)}^{\infty} \mathscr{N}_{\pm} \mathscr{E}^{3/2} (1+\alpha\mathscr{E})^{3/2} \exp(-\lambda^W \mathscr{E})\, d\mathscr{E}, \tag{64}$$

$$a_{12}^{(\mathrm{np})} = \frac{\overline{K}_{\mathrm{np}}}{d_0} \sum_{\pm} \left(n_B + \frac{1}{2} \mp \frac{1}{2} \right) \int_{\hbar\omega_{\mathrm{np}} H(1\mp 1)}^{\infty} \mathcal{N}_{\pm} \mathcal{E}^{5/2} (1 + \alpha\mathcal{E})^{3/2} \exp(-\lambda^W \mathcal{E})\, \mathrm{d}\mathcal{E}, \tag{65}$$

$$a_{21}^{(\mathrm{np})} = \frac{\overline{K}_{\mathrm{np}}}{m^* d_0} \sum_{\pm} \left(n_B + \frac{1}{2} \mp \frac{1}{2} \right) \int_{\hbar\omega_{\mathrm{np}} H(1\mp 1)}^{\infty} \mathcal{N}_{\pm} \frac{\mathcal{E}^{5/2} (1 + \alpha\mathcal{E})^{3/2}}{1 + 2\alpha\mathcal{E}} \exp\left(-\lambda^W \mathcal{E}\right) \mathrm{d}\mathcal{E}, \tag{66}$$

$$a_{22}^{(\mathrm{np})} = \frac{\overline{K}_{\mathrm{np}}}{m^* d_0} \sum_{\pm} \left(n_B + \frac{1}{2} \mp \frac{1}{2} \right) \int_{\hbar\omega_{\mathrm{np}} H(1\mp 1)}^{\infty} \mathcal{N}_{\pm} \frac{\mathcal{E}^{7/2} (1 + \alpha\mathcal{E})^{3/2}}{1 + 2\alpha\mathcal{E}} \exp(-\lambda^W \mathcal{E})\, \mathrm{d}\mathcal{E}. \tag{67}$$

The coupling constants and the values of the phonon energy for each valley are reported in Table 4 [32].

In order to speed up the computation all the integrals giving the expression of U, F, G, C_W and c_{ij} have been evaluated with standard Gaussian quadrature formulas and tabulated versus the energy W. In the numerical code the needed vales of U, F, G, C_W and c_{ij} are reconstructed via interpolation.

References

[1] A. Schenk, Advanced Physical Models for Silicon Device Simulation, Springer, Wien, New York, 1998.
[2] A.M. Anile, V. Romano, Non parabolic band transport in semiconductors: closure of the moment equations, Continuum Mech. Thermodyn. 11 (1999) 307–325.
[3] V. Romano, Non parabolic band transport in semiconductors: closure of the production terms in the moment equations, Continuum Mech. Thermodyn. 12 (2000) 31–51.
[4] V. Romano, Non-parabolic band hydrodynamical model for silicon semiconductors and simulation of electron devices, Math. Method Appl. Sci. 24 (2001) 439–471.
[5] A. Marrocco, A.M. Anile, V. Romano, J.M. Sellier, 2D numerical simulation of the MEP energy-transport model with a mixed finite elements scheme, J. Comput. Electron. 4 (2005) 231–259.
[6] A. Marrocco, P. Montarnal, Simulation des modéles enery-transport á l'aide des èlèments finis mixtes, C.R. Acad. Sci. Paris 323 (1996) 535–541.
[7] A. Marrocco, P. Montarnal, B. Perthame, Simulation of the energy-transport and simplified hydrodynamic models for semiconductor devices using mixed finite elements, in: Proceedings ECOMAS 96, Wiley, London, 1996.
[8] N. Ben Abdallah, P. Degond, On a hierarchy of macroscopic models for semiconductors, J. Math. Phys. 37 (1996) 3306–3333.
[9] R. Stratton, Diffusion of hot and cold electrons in semiconductor barriers, Phys. Rev. 126 (1962) 2002–2014.
[10] D. Chen, E.C. Kan, U. Ravaioli, C.-W. Shu, R. Dutton, An improved energy-transport model including nonparabolicity and non-Maxwellian distribution effects, IEEE Electron Device Lett. 13 (1992) 26–28.
[11] N. Ben Abdallah, P. Degond, S. Genieys, An energy-transport model for semiconductors derived from the Boltzmann equation, J. Stat. Phys. 84 (1996) 205–231.
[12] E. Lyumkis, B. Polsky, A. Shir, P. Visocky, Transient semiconductor device simulation including energy balance equation, Compel 11 (1992) 311–325.

[18] P. Degond, A. Jüngel, P. Pietra, Numerical of energy-transport model for semiconductors with non-parabolic band structure, SIAM J. Sci. Comput. 22 (2000) 986–1007.
[19] S. Holst, A. Jüngel, P. Pietra, Mixed finite-element discretization of the energy-transport model for semiconductors, SIAM J. Sci. Comput. 24 (2003) 2058–2075.
[20] L.D. Marini, P. Pietra, New mixed finite element schemes for current continuity equations, Compel 9 (1990) 257–268.
[21] S. Holst, A. Jüngel, P. Pietra, An adaptive mixed scheme for energy-transport simulations of field-effect transistors, SIAM J. Sci. Comput. 25 (2004) 1689–1716.
[22] V. Romano, 2D simulation of a silicon MESFET with a nonparabolic hydrodynamical model based on the maximum entropy principle, J. Comput. Phys. 176 (2002) 70–92.
[23] A.M. Anile, G. Mascali, V. Romano, Recent developments in hydrodynamical modeling of semiconductors, Mathematical Problems in Semiconductor PhysicsLecture Notes in Mathematics, vol. 1832, Springer, Berlin, 2003.
[24] J.A. Carrillo, I.M. Gamba, A. Majorana, C.-W. Shu, A WENO-solver for the transients of Boltzmann–Poisson system for semiconductor devices: performance and comparison with Monte Carlo methods, J. Comput. Phys. 184 (2003) 498–525.
[25] A. Jüngel, Quasi-Hydrodynamic Semiconductor Equations, Birkhauser, 2001.
[26] D.L. Scharfetter, H.K. Gummel, Large-signal analysis of a silicon read diode oscillator, IEEE Trans. Electron Device ED-16 (1969) 64–77.
[27] A.M. Anile, N. Nikiforakis, V. Romano, G. Russo. Discretization of semiconductor device problems (II), in: Handbook of Numerical Analysis, vol. XIII. Special Volume: Numerical Methods in Electromagnetics, Elsevier, North-Holland, Amsterdam, 2005 (Chapter 5) .
[28] M. Lundstrom, J. Guo, Nanoscale transistor: device physics, modeling, and simulation, Springer, New York, 2006.
[29] J.W. Jerome, C.-W. Shu, Energy models for one-carrier transport in semiconductor devices, in: N.M. Coughran, J. Cole, P. Lloyd, J.K. White (Eds.), Semiconductors Part II, The IMA volumes in Mathematics and its Applications, 1994, pp. 185–207.
[30] S. Selberherr, Analysis and Simulation of Semiconductor Devices, Springer, Wien, New York, 1984.
[31] I.M. Gamba, Asymptotic behavior at the boundary of a semiconductor device in two space dimensions, Ann. Mat. Pura Appl. 163 (1993) 43–91.
[32] C. Jacoboni, L. Reggiani, The Monte Carlo method for the solution of charge transport in semiconductors with application to covalent materials, Rev. Mod. Phys. 55 (1983) 645–705 .